BEARING CAPACITY OF WEB MEMBERS IN FIBER REINFORCED POLYMERIC (FRP) COMPOSITE BRIDGE DECKS

by

Owen K. Silbaugh

B.S., Carnegie Mellon University, 2002

Submitted to the Graduate Faculty of

School of Engineering in partial fulfillment

of the requirements for the degree of

Master of Science

University of Pittsburgh

2004

UNIVERSITY OF PITTSBURGH

SCHOOL OF ENGINEERING

This thesis was presented

by

Owen K. Silbaugh

It was defended on

April 14, 2004

and approved by

Dr. Christopher J. Earls, Associate Professor,
Department of Civil and Environmental Engineering

Dr. Amir Koubaa, Academic Coordinator,
Department of Civil and Environmental Engineering

Thesis Advisor: Dr. John F. Oyler, Adjunct Associate Professor,
Department of Civil and Environmental Engineering

BEARING CAPACITY OF WEB MEMBERS IN FIBER REINFORCED POLYMERIC (FRP) COMPOSITE BRIDGE DECKS

Owen K. Silbaugh, M.S.

University of Pittsburgh, 2004

The primary purpose of this research project is to advance the understanding of fiber reinforced polymeric (FRP) composite bridge deck systems through the study of the bearing capacity of the vertical and offset diagonal webs of a stand-alone, multi-tube FRP composite bridge deck section. The overall rating capacity and ultimate strength capacity of the deck was determined from the testing sequence. The deck was sufficiently strong to withstand AASHTO HS25-44 type loading when tested directly over the vertical and offset diagonal webs. Load versus deflection data was collected for each testing position, and subsequently analyzed and adjusted to reflect assumptions with respect to the beam on an elastic foundation model and the development of the plastic hinge in the HS25-44 steel testing pads. By converting load deflection curves to equivalent stress versus strain curves, the experimental Modulus of Elasticity of each web was determined. In addition, a discussion on the behavior of the FRP panels under the specific testing conditions was presented.

Though the raw data collected from the series of eight bearing tests was not directly comparable, modifications and adjustments were made to remove initial nonlinearities, to replicate the beam on elastic foundation model, and to reflect a hypothetical situation in which all tests were performed with rigid steel test pads. From the adjusted curves, a better understanding of the true behavior of the composite FRP deck under the given AASHTO HS25-

44 loading conditions can be realized and ultimately compared to future studies of the bearing capacity.

TABLE OF CONTENTS

LIST OF TABLES

LIST OF FIGURES

1.0 INTRODUCTION AND BACKGROUND

1.1 RESEARCH MOTIVATION

Design standards for steel, concrete, wood, aluminum, etc. address all possible limit states that might occur in the design process of infrastructure, including bridges, buildings, and roadways. Since these materials, except for wood, have isotropic material and mechanical properties, the formulation of predictive behavioral response equations is simplified. The design process and the establishment of codes and specifications are more complicated with anisotropic materials. Depending on the orientation of the material, the properties can be significantly different. As technology advances within the domain of materials science and engineering, the introduction of new materials into civil engineering practice is expected. One current example of a non-traditional and novel material that has made its way into civil engineering practice is Fiber Reinforced Polymeric (FRP) composites. These new materials present unique challenges to the profession as a result of their lack of homogeneity and isotropy. As more research is conducted to predict and describe the behavior of FRP, design codes, specifications, and guidelines can be established to facilitate the use of FRP in many new areas of civil infrastructure construction and repair.

The primary purpose of this research project is to help move the understanding of FRP bridge deck systems through the study of the bearing capacity of the vertical and offset diagonal

webs of a stand-alone, multi-tube FRP composite bridge deck section. The webs of two identical FRP panels were tested in bearing (see Section 2.2). The first panel tested the vertical web members; the second panel tested the offset diagonal web members. The overall rating capacity and ultimate strength of the panels will be determined from the testing sequence. It is assumed that the webs will exceed the American Association of State Highway and Transportation Officials (AASHTO) HS25-44 design load standards.

From the testing sequence (see section 2.5.2), load versus deflection data was collected (see Appendix B). Each distinct section of the curves will be analyzed to establish an understanding of the behavior of the FRP composite deck section. By converting load deflection curves to equivalent stress versus strain curves, the experimental Young's Modulus (Modulus of Elasticity) of each web will be determined. In addition to the determination of the experimental bearing capacity of each web, a discussion on the behavior of the FRP under the specific testing conditions will be presented.

1.2 INTRODUCTION TO THE USE OF FIBER REINFORCED POLYMERIC COMPOSITES

The Federal Highway Administration (FHWA) released the annual National Bridge Inventory beginning in 1992, detailing the bridge infrastructure in the United States. Of the approximately 590,000 bridges in the latest report, approximately 157,000 were classified as either "structurally deficient" or "functionally obsolete" (FHWA 2003). These classifications do not imply that the bridges are in danger of collapse or failure or otherwise unsafe. Federal, state, and county, transportation agencies are unable to cope with the rate of deterioration of the bridge

infrastructure. Consequently, many states are forced to post load restrictions or even to close bridges as temporary solutions because of budget constraints, until funding comes available to circumvent the situation (Nystrom, et al. 2002).

There is increasing pressure put on transportation agencies to find new construction materials to make bridges cost less to construct and maintain, while increasing their strength and life span. Reduction of the life-cycle costs of bridges decreases the burden placed on transportation budgets and ultimately the taxpayer (Ehlen 1999). One candidate material, made by embedding glass fibers in a polymeric resin, is fiber reinforced polymeric (FRP) composites. Unfortunately, FRP composite bridge decks suffer from: a higher material cost compared to a conventional steel reinforced concrete deck; a lack of quantification of the long term maintenance costs, lack of verification of load-response behavior and durability in various environmental conditions; and the lack of design guidelines, codes, and specifications.

Despite the challenges, FRP composites in construction have a good track record in the United States, Europe, and Japan in the last decade (FHWA 1997). The production and installation of FRP composite panels is not adversely affected by inclement weather conditions, thereby extending construction season well beyond conventional deck placement methods. FRP composite bridge decks possess a high strength-to-weight ratio, making them approximately 80% lighter than conventional steel reinforced concrete decks of the same nominal depth. The use of the lighter FRP decking in bridge retrofit and rehabilitation projects increases the allowable live load capacity of the bridge due to reductions in the dead load to be supported by the existing superstructure. In addition, the lightweight, modular nature of FRP significantly decreases installation time and construction equipment requirements, thus reducing inconvenience to the general public as well as reducing the overall project cost.

Though the long-term durability in various environmental conditions is unknown, FRP provides higher resistance to abrasion, corrosion, and chemical attack than steel reinforced concrete (Scott, Wheeler, 2001). In the wintry northern United States, a substantial portion of concrete deck deterioration can be attributed to the liberal usage of de-icing road salts. FRP composite bridge decks, as compared to conventional concrete decks, appear to be unaffected by road salts, a useful and important feature of this material lending to prolonged service life.

One major problem with FRP composite construction materials, mainly bridge decks, is the lack of published design codes, which would facilitate their day-to-day use. The American Concrete Institute (ACI) has very limited code detailing the use of FRP composite reinforcement in concrete structures. Currently, a code for structures using FRP composites is being developed based on the Load and Resistance Factor Design (LRFD) methodology. In conjunction with the American Society of Civil Engineers (ASCE), AASHTO is developing a standard code for the design of pultruded FRP composite structures (Scott, Wheeler 2001).

Currently, there are fewer than 50 vehicular bridges constructed using FRP composite bridge decks in the United States. In 2001, a partially funded initiative by the Ohio State Legislature was established to replace 100 bridge decks using FRP composite technology (Nystrom, et al. 2002). As many states are increasingly looking for new, cost effective alternatives to replacing conventional concrete bridge decks, widespread use of FRP composites is not far from reality. As it currently stands, FRP composites can be economically justified based on the reduction of life-cycle costs or the reduction of the dead load capacity. Two primary applications for FRP composite bridge decks are the replacement of high-volume deteriorated concrete decks and the rehabilitation of weight sensitive structures (Cassity 2000). With developing technology in the field of fiber composites, the overall cost of pultruding a FRP

bridge section will decrease, making FRP composite decks a viable alternative to conventional concrete decks.

1.3 DESCRIPTION OF FIBER REINFORCED POLYMERIC COMPOSITES

A material aggregate, composed of two or more constituent material components, may be thought of as a composite material. Frequently, composite materials "engineered" in those favorable qualities from each of the component materials are exploited within the context of the dominant behavioral features of the other materials in the material system. In the case of fiber reinforced composites, reinforcing strands exhibiting important strength and stiffness properties are oriented and carefully positioned with respect to each other through the use of a polymeric matrix that provides some mechanical strength as well as providing protection from environmental attack. Within the context of fiber reinforced composite materials, one layer of composite material is defined as a lamina; stacking multiple laminae forms the laminate (Austin 2002). The designation FRP is given to any number of advanced composite materials consisting of two primary constituents, fiber reinforcement and a polymer matrix (Luo, et al. 2002). Other constituents, fillers and additives, can be added to the composite. While the resin acts as the "glue" to hold the composite together, the fillers and additives aid in providing corrosive resistance, UV radiation protection, and serve other important functions in the material. Because of the inherent anisotropic nature of FRP composites, the overall properties of the laminate are directional. Loading parallel to the fiber direction provides the best mechanical properties. Orienting glass fibers with respect to one another and subsequently wetting and

impregnating these fibers with an iso-polyester base thermoset resin that is subsequently heated to facilitate hardening leads to a FRP laminate. These same constituent materials in the composite system can be combined using pultrusion, a manufacturing technique most frequently utilized in advanced civil engineering composites. Pultrusion is a very similar process to that previously described for the construction of an FRP laminate; the only difference is that instead of a flat laminate being the end results, a structural cross-section or shape is produced.

The primary function of the fiber reinforcements is to carry the load and provide strength and stiffness in the FRP laminate. Typically, fiber reinforcement is oriented at 0, ±45, and 90 degrees to the direction of pultrusion, though orientation can be customized to provide sufficient properties in the direction of the explicit loads for a particular design application. The reinforcement can be made from glass, carbon, or aramid fibers. Produced from alumina-lime-borosilicate composition, E-glass fibers are the most common types of reinforcement because of their useful mechanical properties and low susceptibility to degradation from weathering and chemicals (MDA 2000). Another type of glass reinforcement is S-glass, which has higher strength, heat resistance, and cost. Compared to glass fibers, carbon fibers are more expensive, though lighter, and have a higher modulus of elasticity. Aramid fibers are man-made and offer low density with high impact resistance and a modulus of elasticity that is 1.5 times that of glass fibers (MDA 2000).

Reinforcing fibers in FRP composites can be rovings, continuous strand mats (CSMs), or stitched or woven fabrics. There are two types of rovings, multi-end and single-end. Multi-end rovings consist of many strands of filaments, which are chopped and randomly placed in a solid matrix. For single-end rovings, filaments are wound to form a single strand. Stitched or woven fabrics are supplied on rolls that vary in length and width and are robust enough to be handled,

while at the same time being malleable enough to conform to dies or molds. For the woven fabric, the fibers oriented at 0 and 90 degrees are woven together to form the fabric. The stitched fabric has fibers oriented in collections at 0, ±45, and 90 degrees. Each layer of fibers is crimped and sewn together. CSMs have randomly oriented fibers like rovings but are produced in rolls like a fabric. In this thesis, E-glass fibers with the following properties will be considered (Austin 2002):

$E_f \equiv$ Modulus of Elasticity of Fibers= 10,500 ksi

$\upsilon_f \equiv$ Poisson's Ratio of Fibers = 0.22

$G_f \equiv$ Shear Modulus of Fibers = 4,300 ksi

A low strength, solid matrix composed of resin protects the fibers from mechanical and environmental degradation in addition to transferring stress between reinforcement by bonding the E-glass fibers together. There are two main groups of resins: thermosetting and thermoplastic. The most common, widely used, and cost effective are thermosetting resins, which include polyesters, epoxies, and vinyl esters. Polyester resins can be customized to meet application requirements and are said to have "balanced" properties (mechanical, electrical, and chemical) (MDA 2000). With high mechanical and electrical properties, excellent performance in high temperatures and corrosive environments, and good adhesion to substrate, epoxy resins are used for high performance composite application. The viscous nature of epoxies requires elevated heat and longer curing time to achieve the greatest mechanical properties. Vinyl ester resins can be used to improve curing time and decrease viscosity as compared with standard

polyester resins. The type of polyester resin used in the deck sections in this thesis is proprietary, with the following assumed properties (Austin 2002):

E_r ≡Modulus of Elasticity of Resin= 500 ksi

υ_r ≡Poisson's Ratio of Resin = 0.38

G_r ≡Shear Modulus of Resin= 180 ksi

Pultrusion combines the fiber reinforcement and thermosetting resins in a continuous molding process. Pultruded FRP shapes can be manufactured for any prismatic cross section. The pultrusion process consists of pulling rovings, CSMs, resins, and the thin mat, surfacing layer (nexus) through a resin bath that wets and impregnates the fibers with the polyester resin (Austin 2002, MDA 2000). Subsequently, the saturated fibers are pulled through a heated steel die in the shape of the desired cross section. Chemical reactions take place in and around the fibers thus leading to the formation of a hardened matrix (Luo, et al. 2002). The continuous nature of the pultrusion process allows cross sections to be cut to the desired width. Schematics of the pultrusion process are presented in Figures 1.1 and 1.2. The FRP composite bridge decks used in experimental testing were supplied by Martin Marietta Composites and were manufactured by Creative Pultrusions, Inc. using the aforementioned pultrusion process.

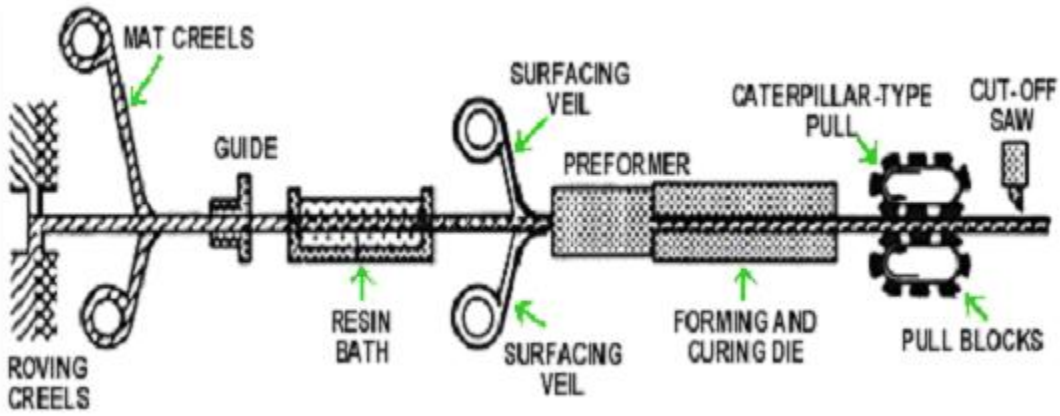

Figure 1.1 Schematic of Pultrusion Process

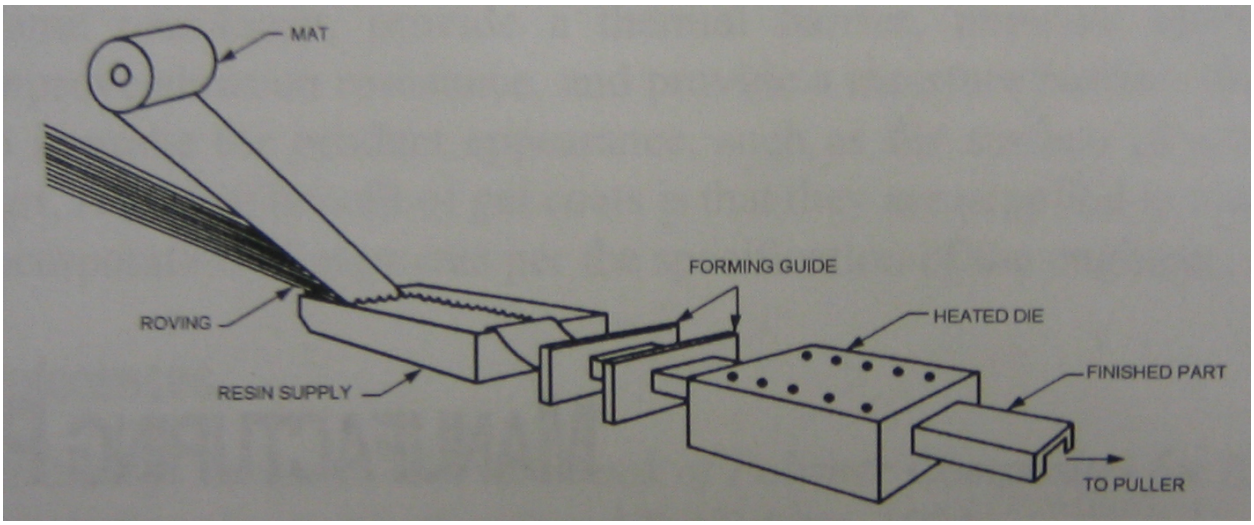

Figure 1.2 Schematic of Pultrusion Process (Courtesy of MDA 2002)

1.4 THESIS ORGANIZATION

The organization of this thesis is divided into five chapters. Chapter 1 details background information related to FRP manufacturing and application. The test specimens, equipment, and procedure are described in Chapter 2. A discussion of the data collected is presented in Chapter 3. Chapter 4 explains and analyzes the load versus deflection data and presents conclusions. In Chapter 5, recommendations for future research are presented. In the appendices, the actual and adjusted load versus deflection curves are presented along with the development of the plastic hinge in the "flexible" plate and the beam on elastic foundation model.

2.0 BEARING CAPACITY TESTS

2.1 INTRODUCTION

As the infrastructure in the United States continues to deteriorate, FRP composite bridge decks are a viable alternative to conventional reinforced concrete decks. Before codes, guidelines, and specifications for the use of FRP in construction are created and put into widespread use, experimental testing must validate theoretical calculations and load behavior response must be completely understood. Currently, experimental research is being conducted at numerous universities sponsored by state highway departments and composite material manufacturers. In this chapter, a detailed description of the composite FRP bridge deck specimens, steel loading pads, and test equipment used for the bearing capacity tests is presented. In addition, a description of the test setup, including testing positions, testing procedure, problems encountered, and how they were circumvented, is provided.

2.2 FRP COMPOSITE BRIDGE DECK PANELS

Two identical DuraSpan^{TM} 500 bridge deck panels were supplied by Martin Marietta Composites to be tested in the Watkins-Haggart Structural Engineering Laboratory at the University of Pittsburgh. The bridge decks were manufactured at Creative Pultrusions, Inc. Each of the sample deck panels was fabricated from three pultruded tube cross-sections that were bonded together along two joint interfaces using an epoxy adhesive.

Each of the six tube sections of the two bridge decks was pultruded in six-foot widths. The pultruded direction was assumed to be perpendicular to the direction of the traffic flow in an actual field installation. The cross section of one tube section of the deck contained of four identical trapezoidal voids. As seen in Figure 2.1, the tube section was made up of one open cell and four closed cells.

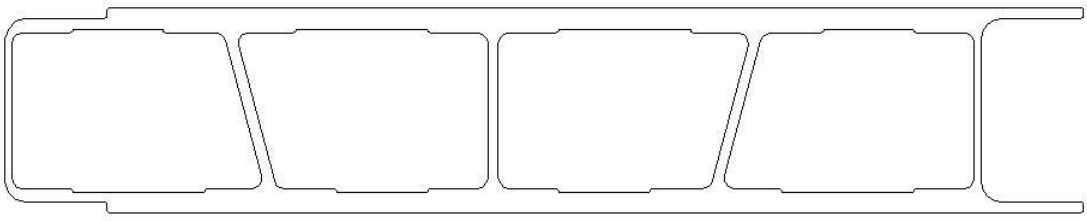

Figure 2.1 Typical Cross Section of One FRP Bridge Deck Tube Section

The completed deck specimens measured about 6.25 feet in length, 6 feet in width, and 5 inches thick after fabrication (see Figure 2.2). The center vertical web and the two offset diagonal webs were about 1/4 inch thick. The end vertical webs were about 5/32 inch thick. At the junction where two panels were bonded together, the thickness of the vertical web was about 10/32 inch; this measurement did not account for increased thickness due to the bonding agent. The thickness of the top and bottom flanges varied, approximately, between 1/2 inch and 5/8 inch. At the end with the open cell section, the thickness of the flanges was about 3/16 inch. The thickness of the flanges of the tapered section at the end opposite the open cell section was about 13/32 inch. All edges were filleted to minimize stress concentrations. See Table 2.1 for a summary of the aforementioned data. Figure 2.3 displays one tube section with dimensions (note all measurements given as nominal).

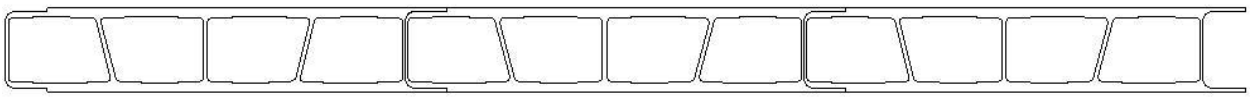

Figure 2.2 Cross Section of a Multi-tube DuraSpan™ 500 Test Bridge Deck Panel

Table 2.1 Summary of Nominal Thicknesses of DuraSpan™ 500 Deck

Member Type	Thickness [inches]*	Member Type	Thickness [inches]*
Inside Vertical Webs	1/4	Top & Bottom Flanges	1/2 – 5/8
Tapered End Vertical Webs	5/32	Open Cell Flanges	3/16
Open Cell Vertical Webs	5/32	Tapered Flanges	13/32
Bonded Vertical Webs	10/32	Offset Diagonal Webs	¼
* – All values are nominal			

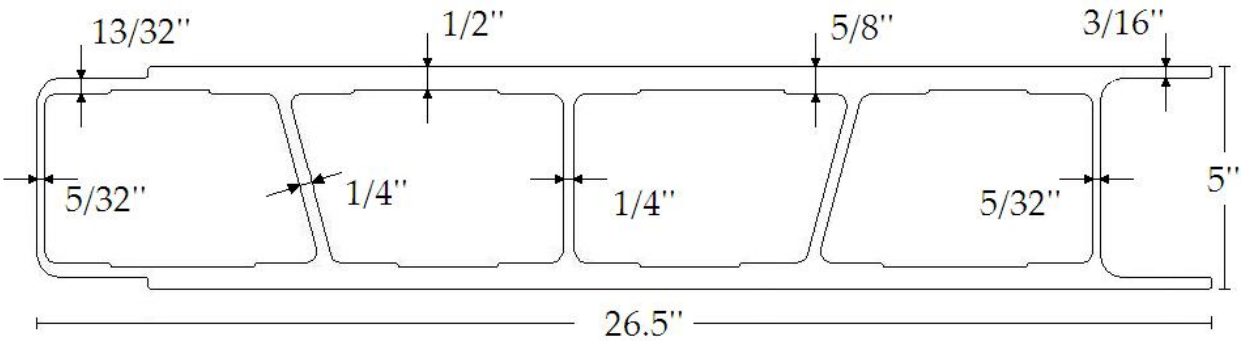

Figure 2.3 Dimensioned Cross Section of a Single FRP Tube Section

2.3 STEEL TESTING PADS

Since the objective of this research was to evaluate the bearing capacity of individual web elements within the pultruded cross section when loaded in bearing, a realistic bearing loading was sought. It was decided that a tire patch consistent with an AASHTO HS25-44 design vehicle was a reasonable choice. As the geometry and orientation of the various cross-sectional web changed with location within the deck specimens, several different loading positions were considered. For each loading position, the steel loading pads were chosen according to AASHTO Standards and specifications provided by Martin Marietta Composites. The thickness of the pads for the offset diagonal webs was changed because of problems encountered during the vertical web tests (see Section 2.6.2). For consistency in test results from all research of FRP composite bridge decks sponsored by Martin Marietta Composites, the footprint (10 inches by 20 inches) was used to simulate the tire loads of a typical AASHTO HS25-44 truck.

Currently, AASHTO does not require HS25-44 design loading and has no current specification to govern this standard. The Texas Department of Transportation (TXDOT) has designed bridges along the Texas-Mexico border using the HS25-44 design specification to accommodate international truck traffic (TXDOT 2001). See Figure 2.4 for the typical HS15-44 and HS20-44 design truck with tire loads (AASHTO Design Manual 1996). Comparable loads for an HS25-44 truck should be 10,000 pounds, 40,000 pounds, and 40,000 pounds, respectively, for the axles as pictured in Figure 2.4. Where W is equal to 50,000 pounds for the HS25-44 truck, therefore the design wheel load is 20 kips on each side of the rear two axles.

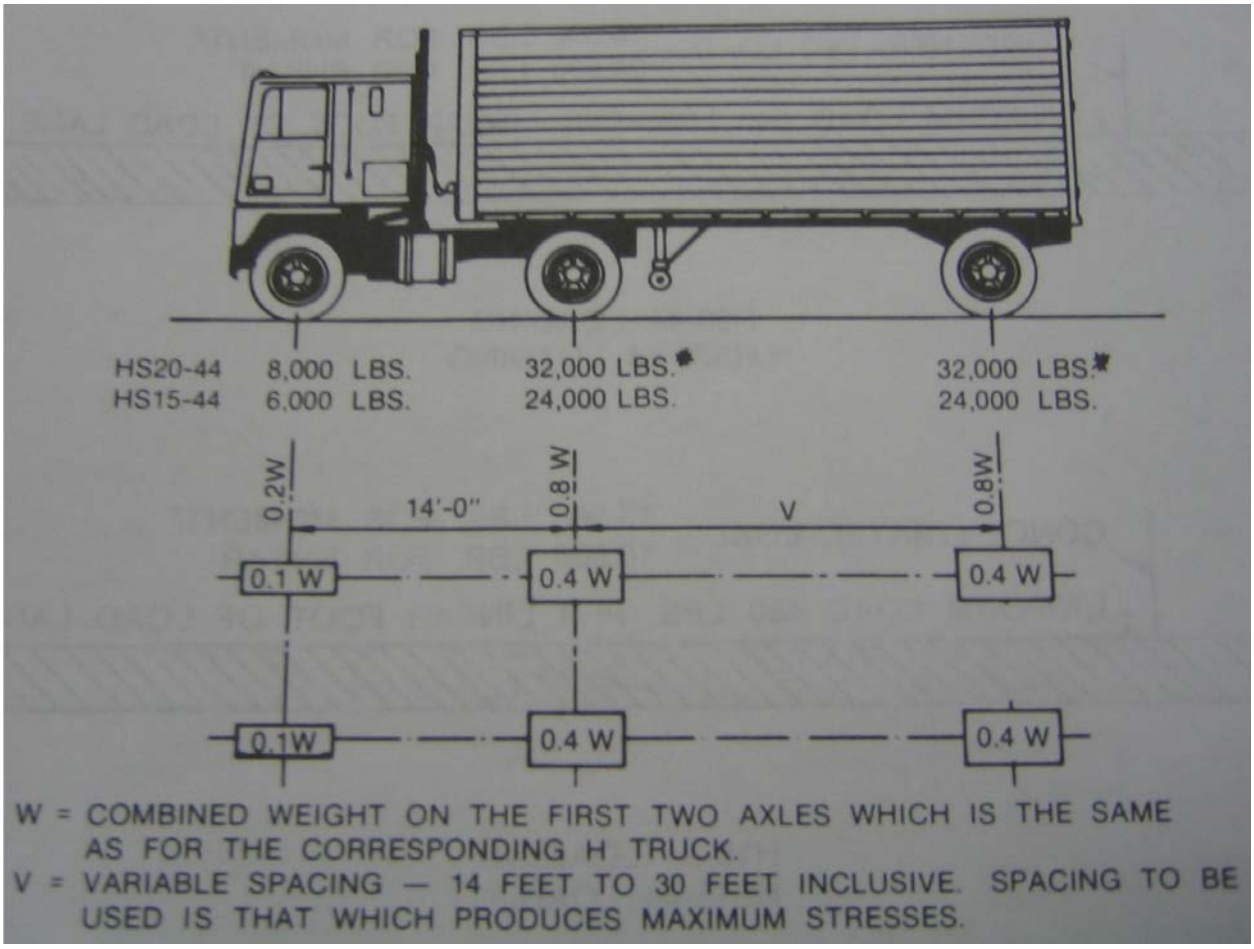

Figure 2.4 HS15-44 and HS20-44 Design Truck With Tire Loads (AASHTO 1996)

Two different pad thicknesses were used during the testing of the two test deck specimens: one-inch ("flexible") plates for the vertical web tests and three-inch ("rigid") plates for the offset diagonal web tests. Both the flexible and rigid plates had the same footprint and were assumed to be A36 Grade steel. The actual grade of steel is unknown because coupons were not tested for this plate stock. The thickness of the flexible plates was one inch, whereas

the rigid plates were three inches. A different plate was used for each loading position for both FRP deck panels. Welded to each plate was a ten inch long and 2 inch diameter piece of steel rod. The orientation of the rod was parallel to the direction of traffic and centered on each plate (see Figures 2.5 and 2.6).

Figure 2.5 The One-inch Thick Steel Test Pads Used For Testing Positions 1 Through 5

Figure 2.6 Three-inch Thick Steel Test Pad

2.4 TESTING EQUIPMENT

In this section, a description of the testing equipment will be presented, including the components of the data collection system, loading system, and the load frame. The type and model of each piece of equipment, used in the current research, is provided. For a complete understanding of the test setup, the assembly of the load frame is important.

2.4.1 Data Collection System

The main component of the data collection system was the direct current displacement transducer (DCDT), which measured the displacement of the FRP deck panel. The DCDT was connected to the data acquisition system, which was a 90 channel Vishay-Micro Measurements System 5000. Since only one DCDT was used (to measure actuator motion) only one channel was utilized per loading sequence. The data acquisition system was connected to a computer running the StrainSmart computer program.

2.4.2 Loading System

One 200 kip hydraulic actuator was connected to the columns and crossbeam as discussed subsequently in section 2.4.3. The actuator is a MTS fatigue rated with a Moog servo-valve with capacity of 60 gallons per minute. The 60 gallons per minute Sauer-Sundstrand Pump in the Edison Hydraulic Pump unit supplies the actuator with sufficient hydraulic capacity. A 200 kip Strainsert load cell was attached to the actuator and wired to a card on a MTS 458 with a Micro-Profiler. See Appendix A for pictures.

2.4.3 Load Frame

The load frame consisted of two parts: the frame section carrying the actuator and the load section (i.e. main beams, etc.) that supports the frame section. The load frame was assumed to be stiff enough that objectionable deflections were not experienced when the actuator was applying loads to the test specimens. See Appendix A for pictures.

The total dimensions of the load frame are 34 feet in length and 8 feet in width, though only a small percentage of the length was utilized for the bearing test (see Figures A 1 and A 2). The first component of the load section is the main beams, which consist of the two built-up wide flange sections, which are supported by the reaction floor. The second component of the load section consists of the diaphragm bracing beams, which are built-up wide flange sections. The diaphragm bracing beams are connected to the web of the main beams. The frame section consists of two columns and a crossbeam. The columns are bolted to the top flanges of the main beams, and the crossbeam is bolted to the columns at the desired location. The actuator and load cell are bolted, via large plates, to the underside of the bottom flange of the crossbeam. The columns and crossbeam loading system can be easily moved to accommodate the different loading positions for each test of the respective FRP decks.

The two main beams are built-up sections made from a 30WF172 (34 feet in length) that rest on the reaction floor, with one-inch thick steel cover plates welded to the top and bottom flanges. The main beams are connected via the three diaphragm bracing beams (30WF172, six feet in length), which are web-bolted to the full-depth web stiffeners of the main beams at each connection point. The diaphragm bracing beams are spaced eight feet, center-of-web to center-of-web, with the middle diaphragm seventeen feet from each end of the length of the main beams. The bearing tests were performed between two of the diaphragm beams (the importance of this will be explained later in Section 2.5.1). Two rows of one-inch diameter holes spaced six inches center-to-center along the respective lengths of the top flanges of the main beams and the diaphragm bracing beams (i.e. all 30WF172 beams) are provided so the columns of the loading system can be properly secured with high strength bolts.

The columns supporting the crossbeam and actuator are 12WF85 sections, 12 feet in length. For the bearing test, two columns and a single crossbeam are used. Welded to the bottom of each of the columns is a thick base plate (15 inches by 22 inches by 2.5 inches), which is used to attach the columns to the top flanges of the main beams using high strength bolts and the aforementioned holes. In addition, there are two rows of one-inch diameter holes spaced three inches center-to-center along the top and bottom flanges of the columns. The crossbeam is a built-up section that forms into a box cross-sectional shape. The plates that make up the flanges are 1.5 inches thick, 20 inches wide, and 7 feet long; the plates the make up the webs are 0.75 inches thick, 17 inches wide, and 9 feet long. The additional length of the web plates is to accommodate the overlap that is needed to permit bolting the crossbeam section to the flanges of the columns. The extended sections of the web plates also have boltholes that align with the boltholes of the column. Attached to the underside of the crossbeam is the actuator and load cell.

The built-up box-shaped crossbeam is constructed with the vertical plates inset 1.5 inch from the edge and welded to the top and bottom plates. The 1.5-inch lip accommodates the secure attachment of the actuator to the crossbeam. Three steel plates, two random-sized pieces of steel, and high strength bolts make up the attachment mechanism for the actuator. One of the three steel plates measures 24 x 24 x 1.5; the other two have dimensions of 24 x 4.5 x 1.5. Both small plates have 1 inch bolt holes spaced 4 inches center-to-center, wherein the larger plate has the same size bolt holes and spacing along two opposite edges and in the middle of the plate that align for connection of the actuator. The actuator is attached to the large plate via high strength bolts. The smaller plates rest on the lip on each side of the crossbeam. Aligning the boltholes in the larger and smaller plates, high strength bolts are used to connect the actuator and plates to the crossbeam. Two small pieces of steel are placed between in the space between the larger and

smaller plates on each side to prevent the twisting of the smaller plates and to help secure the actuator to the crossbeam. The load cell and foot are attached to the actuator by a large finely threaded rod. See Appendix A for figures and pictures.

2.5 TEST SETUP

The purpose of the experimental testing is to analyze, understand, and reflect on the collected data. When new materials like FRP are being tested under specific conditions, it is important to understand the exact setup of each test, such that future research can be conducted under the same conditions. In addition, a description of the initial setup was important such that changes could be made to circumvent unforeseeable problems. In the following section, details describing the insight into the initial setup conditions and the specific testing positions and testing order for each of the FRP bridge deck panels are presented.

2.5.1 Initial Setup

Because of the nature of the testing, the load frame had to be secured to the reaction floor to prohibit uplift. The FRP sample test bridge decks were tested while laying flat on the rigid laboratory reaction floor (thus fully supported over their surface), which is 24 inches thick of concrete reinforced with steel bars. There are holes 2.5 inches in diameter through the thickness of the reaction floor, spaced 18 inches center-to-center around the area of the load frame. To

secure the load frame to the reaction floor, threaded rods, large nuts, washers, and HSS8x8 (14 feet in length) steel tubes were used. Two and a half inch diameter holes were flame cut from the top and bottom of each side of the tube steel, such that the holes aligned with the holes in the reaction floor. The tubes were oriented perpendicular to the direction of the length of the main beams and placed on the top flanges of the main beams spanning beyond the eight-foot width of the load frame adjacent to the point of loading (see Figure A 1). The tubes were extended past the outer the part of the main beams to accommodate alignment with the tie-down holes in reaction floor. The threaded rods were placed through the holes in the tube steel and the reaction floor. High strength nuts and washers were placed on both sides of the reaction floor and on the topside of the tubes, to secure the load frame to the reaction floor.

Using a crane, the FRP test deck was lowered into position between the two diaphragm bracing beams. The deck was centered between the two main beams and aligned with the centerline of the actuator and columns. Because of the nature of the test, the deck had to be secured to the reaction floor to prevent shifting during testing. Two W8x10 bracing beams (7.5 feet in length) were placed along the edges of the deck perpendicular to the diaphragm bracing beams. The bracing beams extended from web to web of the diaphragm bracing beams. Each end of the bracing beams was directly under the top flange of the diaphragm bracing beam. Placing a piece of threaded rod with nuts at each end between the topside of the top flange of the bracing beam and the underside of the top flange of the diaphragm bracing beam and tightening, fixed the two parallel boundaries of the FRP bridge deck, which were subsequently braced and shimmed against the bottom side of the top flange of the diaphragm bracing beams.

Once the FRP bridge deck was in position, the columns carrying the actuator were aligned with the centerlines of the plate and bolted to the top flange of the main beams. The steel test

pad was aligned with the centerlines of the columns and actuator over the desired web to be tested within the footprint drawn on the deck panel. A DCDT was attached to the actuator, in-line with its motion, using clamps and magnets (see Figure A 9). Using a plumb bob, the DCDT arrangement was made to be vertically plumb. Before the loading sequence began for each position, the DCDT reading was "zeroed" in the StrainSmart program. See Figure 2.7 for the setup before testing of loading position 5.

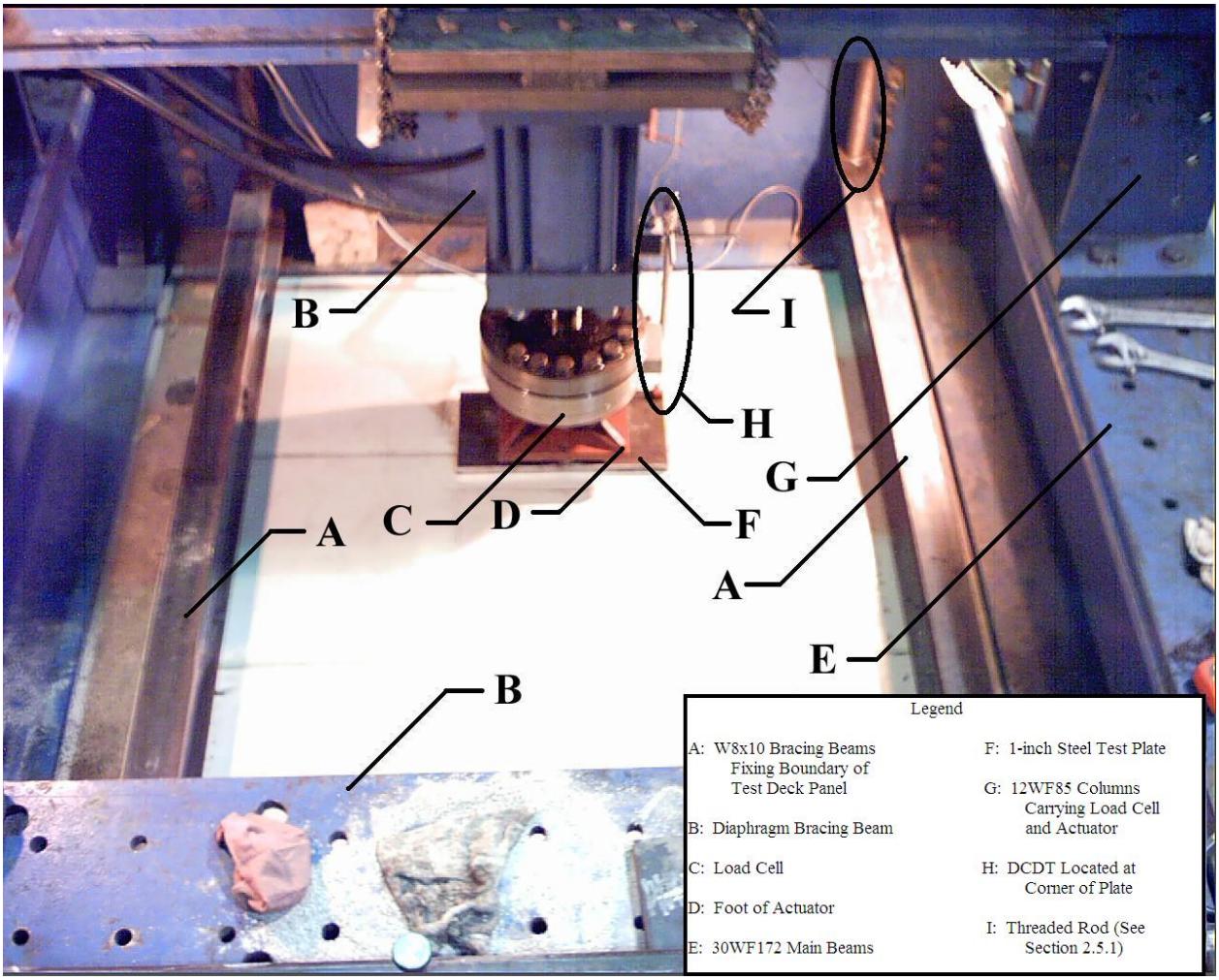

Figure 2.7 Test Setup Prior to Loading of Testing Position 5

2.5.2 Loading Positions

In accordance with correspondence and specifications provided by Martin Marietta Composites, the loading positions were established. Different loading positions were selected for the two test deck panels. The purpose of the test program was to determine the bearing capacity of the vertical and offset diagonal webs. The loading positions for the tests are numbered one through nine; positions one to five for the vertical web tests and six to nine for the offset diagonal webs. The numbering denotes the order of testing. See Figure 2.8 for representative test layout of footprints drawn on the top of the FRP test deck prior to testing.

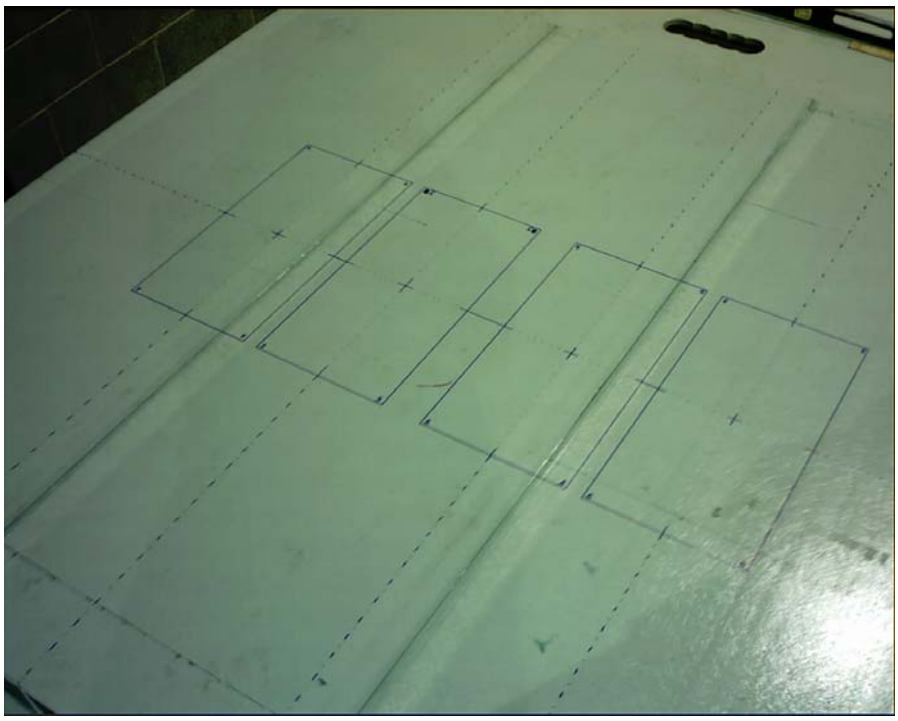

Figure 2.8 Representative Layout of For the Placement of the Steel Test Pads Prior to Testing

The testing locations for the first deck panel specimen were positioned over the vertical webs. Testing locations, one through three, were positioned over the interior vertical webs of each tube section. Testing positions four and five are situated over the vertical webs that are comprised of the bonded area of two tube sections. See Figure 2.9 for comprehensive visual of loading sequence and position for the first test panel.

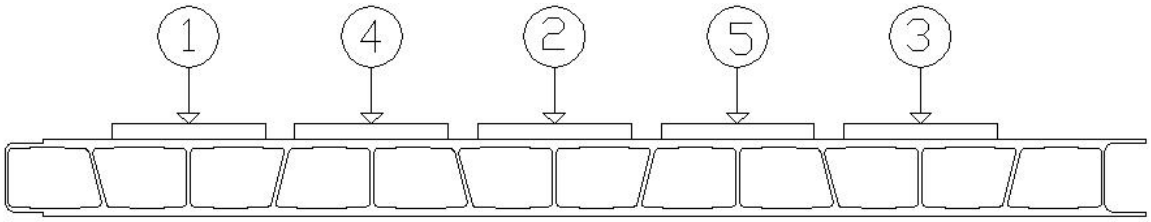

Figure 2.9 Loading Sequence and Positions For Vertical Web Members

For the second panel, the testing locations were positioned over the offset diagonal webs (testing positions six through nine). Positions six and seven were +α degree diagonal webs; positions eight and nine were –α degree diagonal webs (nominal value of α is 115º). See Figure 2.10 for a comprehensive visual of the loading sequence and positions for the second test panel, and see Figure 2.11 for a depiction of the measurement of the angle, α.

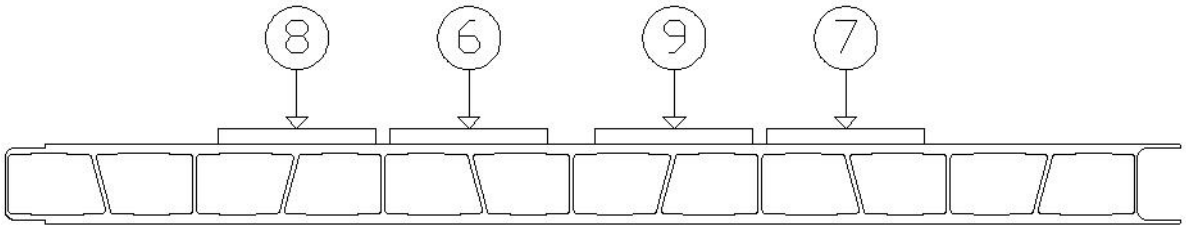

Figure 2.10 Loading Sequence and Positions For Offset Diagonal Web Members

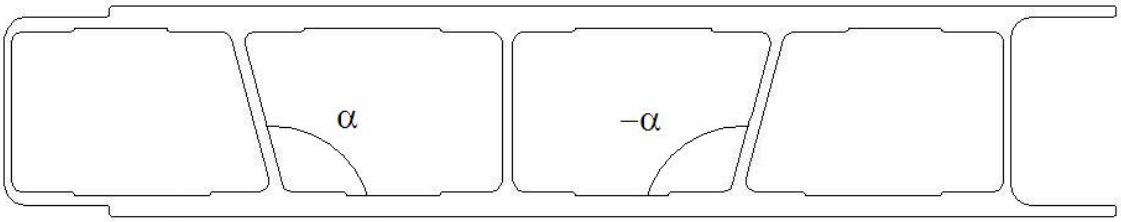

Figure 2.11 Depiction of Angles

The locations of the testing positions were discussed with respect to the deck length and orientation over the vertical and offset diagonal webs. The testing positions are centered with respect to the width of the panel. See Figures 2.12 and 2.13 for a three-dimensional view of the testing positions; the dark gray rectangular solids represent the steel test pads.

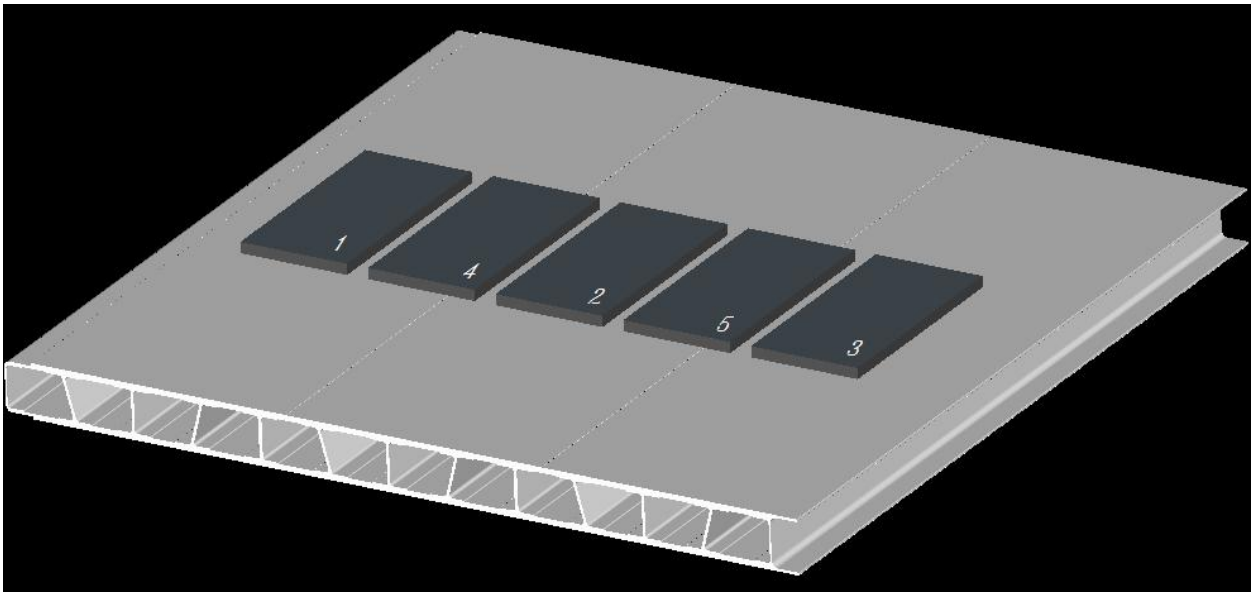

Figure 2.12 Three-dimensional View of First Deck (Vertical Web Members)

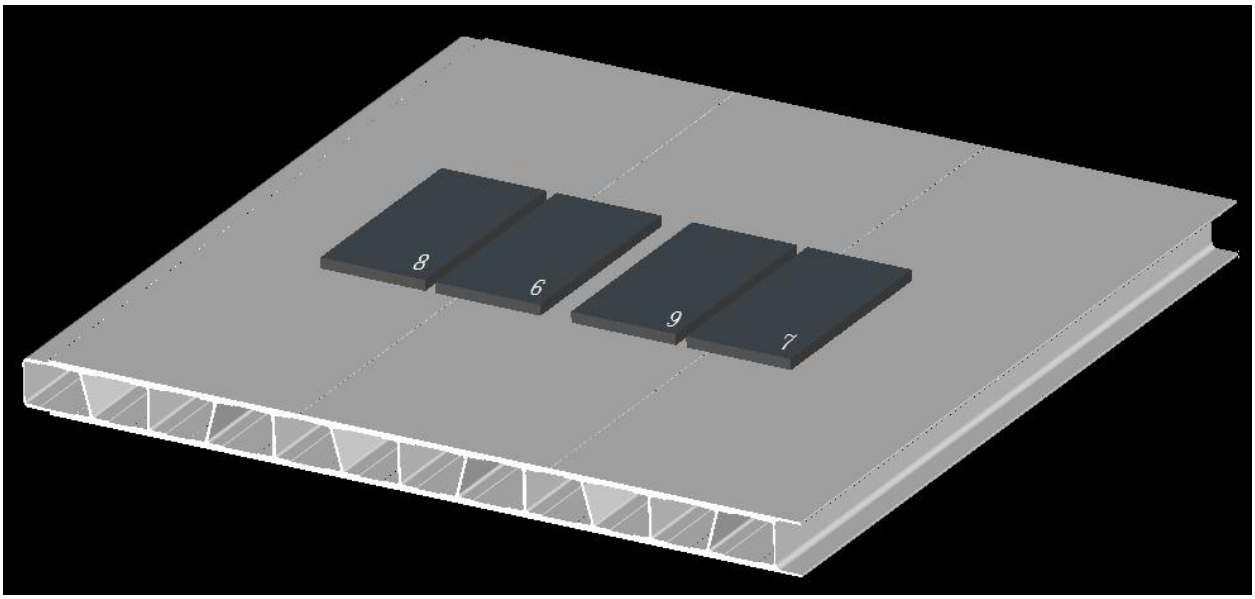

Figure 2.13 Three-dimensional View of Second Deck Panel (Offset Diagonal Web Members)

The possibility of damage spreading to other testing positions was anticipated prior to testing of the first test deck panel. According to Martin Marietta Composites, the possibility existed that positions 4, 5, 8, and 9 would not be tested. For the first five testing positions (i.e. vertical webs), there was very little visual evidence of residual damage effects on the subsequent testing positions; thus all were tested. This was not the case for the next four testing positions, because of a decision to alter the thickness of the steel test pads from one inch to three inches (see Section 2.6.2). Subsequently, tests six and seven caused significant damage such that it was obvious that tests eight and nine should not be performed. In Figure 2.14 (position 6), the top of the three-inch thick steel pad was flush with the top of the FRP deck after loading and ultimate failure (position 7 had a similar configuration). Part of the test pad was situated over a bonded joint, and there was significant debonding of the joint after failure.

Figure 2.14 Damage Caused By the Embedded Steel Test Pad After Completion of Test 6

2.6 TESTING PROCEDURE

Much important information and insight into uncharacterized behavior, giving validation to theoretical formulations, comes from experimental testing. At the time this research was conducted, the bearing capacity tests were the first of their kind. With any new test, there will be unforeseeable problems with the testing method, either during the testing or after the testing

when the data is being analyzed. In the following section, the replication of the testing procedure and the problems encountered are presented.

2.6.1 Execution of Loading

After the displacement measurement on the DCDT was zeroed, the testing sequence began. In approximately two kip per minute intervals, the deck was loaded, and displacement measurements were recorded via the computer program StrainSmart. The load and corresponding deflection values were entered into a spreadsheet. Loading continued though the design load (AASHTO HS25-44) to ultimate failure of the deck. The applied load was immediately removed, and the setup sequence for the next testing position began.

2.6.2 Problems Encountered

With any new test there are problems that occur, mostly unforeseeable problems. During the testing of the first deck (i.e. vertical web tests, positions one through five), there was a problem with the AASHTO HS25-44 test pads. The one-inch thick plates sustained significant permanent deformation after the testing sequence was completed for testing positions 1, 2, and 3; positions 4 and 5 had no visible permanent deformation. This could be explained by the fact that the ultimate loads were significantly lower.

The purpose of the steel test pad was to simulate the tires of an HS25-44 truck. Since the plates deformed, the test pad essentially did not perform its intended function of spreading the load evenly over the contact surface with the deck. Instead of being a uniform distributed load

over the entire area of the test pad, a small concentrated line load was developed in the center of the plate across the ten inch width.

To correct the development of the plastic hinge in the steel test pads encountered during the testing of the first FRP deck panel, three-inch thick plates was used for the second FRP deck panel. The thicker plate had 27 times the flexural rigidity of the one-inch plate. During the testing of position 6 (offset diagonal webs), there was a problem with the load frame lifting off the reaction floor. The occurrence of this can be coupled with the fact that steel loading pad was not permanently deforming, creating a uniform distributed load over the entire area of the test, enabling the applied load to be distributed over a large portion of the web and flanges. It is suspected that the deflection data was significantly altered due to the frame lifting off the floor. As soon as it was realized that the uplifting force from the applied load was greater than moment arm of the weight of the load frame, testing was immediately stopped.

To circumvent this problem the load frame was secured to the reaction floor on the other side of the point of load application. Again an HSS8x8 (14 feet in length) along with threaded rods, nuts, and bolts was used to secure the load frame to the reaction floor as described earlier (see Figure A 1). Since position 6 was stopped prematurely (now denoted test 6a), it was retested as test 6b (fully restrained). These notations are the same on the load versus deflection curves found in the appendices. Test position 7 was tested under fully restrained conditions. See Section 3.5 for further discussion of the lifting of the load frame.

3.0 ANALYSIS OF RESULTS

3.1 INTRODUCTION

The focus of this chapter is the presentation and analysis of the results from the load bearing tests of the web members. A brief summary of the design load capacity and ultimate load capacity is presented. The load versus deflection data is analyzed; each particular portion of the curves is dissected, discussed, and subsequently transformed into equivalent stress strain relationships. As mentioned in the Section 2.6, the testing conditions for each FRP composite panel were considerably different. The vertical webs (loading positions 1 through 5) were all tested in a partially restrained configuration (see Figure A 1) using a one-inch (flexible) steel test pad; the data collected from these tests can be compared. The offset diagonal webs (loading positions 6 through 9) were tested in both partially restrained and fully restrained (see Figure A 2) configurations using a three-inch (rigid) steel test pad. Loading positions 8 and 9 were not tested due to significant damage caused by the failure of the testing positions 6 and 7 (see Section 3.7). Position 6 was tested twice because the load frame began to lift off the reaction floor at an applied load of approximately 96 kips. For testing position 6, 6a denotes the partially restrained condition of the initial test, whereas 6b denotes the retest under the fully restrained condition. The testing conditions for position 7 were fully restrained. See Table 3.1 for a summary of the testing conditions for each composite FRP panel. For all of the testing positions, the deflection

readings were measured at the corner of the steel plate. The load deflection curves were adjusted to reflect the actual deflections at the center of the one-inch plate with respect to Hetényi's beam on elastic foundation model (see Section 3.5). For the tests using the rigid plates, the change in the deflection measurements at the corner of the plate compared to the actual deflections at the center of the plate was negligible due to the increased flexural rigidity of the three-inch plates. For all the testing positions, the load deflection curves were adjusted to reflect the correction of the initial nonlinear behavior at the start of load application. Finally, using Hetényi's beam on elastic foundation, a hypothetical model adjusting the thickness of the one-inch steel test pad to three inches and a discussion of the probable failure modes is presented. Figure 3.1 is a representative unadjusted load deflection curve for testing position 2 with descriptive labels and terminology that will be used herein.

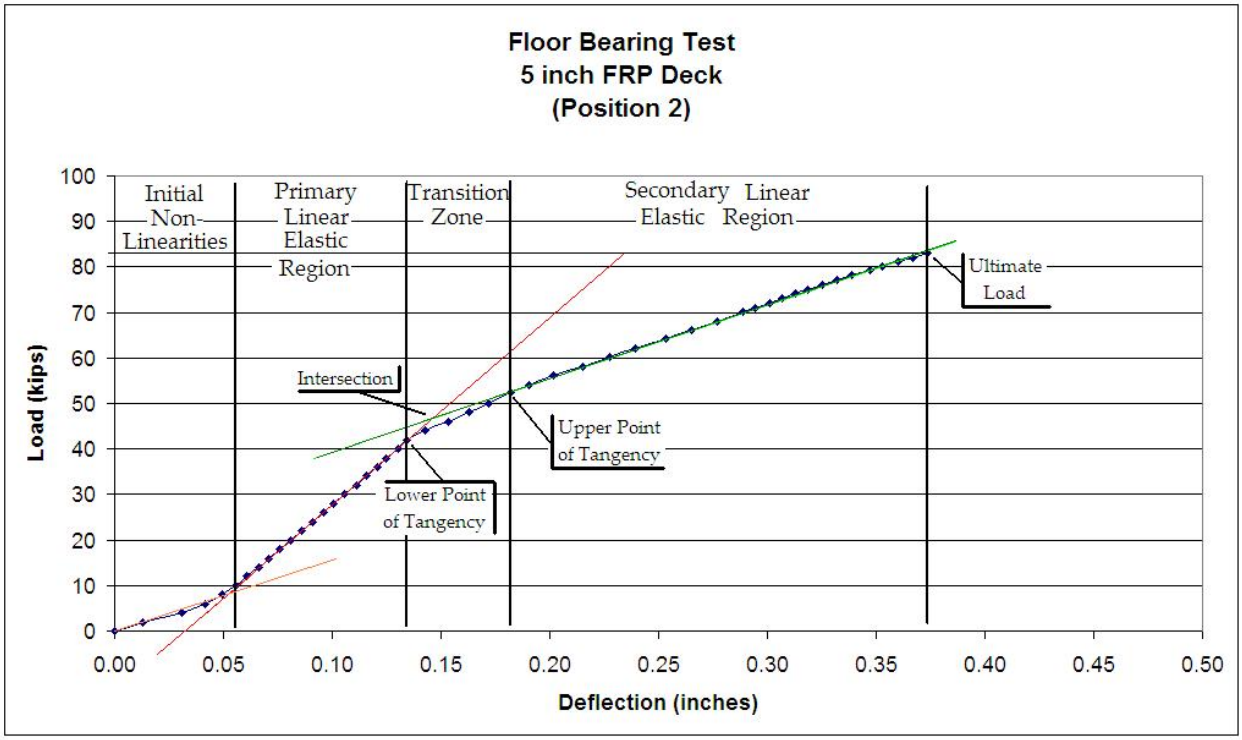

Figure 3.1 Representative Load Deflection Curve For Testing Position 2

Table 3.1 Summary of Loading Plate Type and Restraint Configuration

Test Number	Deck Panel Number	Web Type	Plate Type	Restraint Config-uration	Tested Over a Joint	Influences[g]
1	1	Vertical	Flexible[a]	Partially[c]	No	No
2	1	Vertical	Flexible	Partially	No	No
3	1	Vertical	Flexible	Partially	No	No
4	1	Vertical	Flexible	Partially	Yes[e]	Yes
5	1	Vertical	Flexible	Partially	Yes	Yes
6a	2	Diagonal	Rigid[b]	Partially	Partially[f]	No
6b	2	Diagonal	Rigid	Fully[d]	Partially	No
7	2	Diagonal	Rigid	Fully	Partially	No

a – Denotes 1 inch thick steel test pad was used

b – Denotes 3 inch thick steel test pad was used

c – See Figure A 1 for depiction of the partially restrained configuration

d – See Figure A 2 for depiction of the fully restrained configuration

e – The test position was directly over a joint

f – Only a small portion of the 20 inch length of the plate was positioned over the joint

g – Ultimate strength of testing position possibly compromised by previously failed positions

3.2 DESIGN LOAD CAPACITY

The experimental design load capacity for each of the web members tested was dictated by the AASHTO HS25-44 load rating capacity. The specification from Martin Marietta Composites called for a steel test plate of dimensions 20 inches by 10 inches by 1 inch (see Section 2.3). The purpose of the test pad was to simulate the tire contact area of two adjacent wheels of an HS25-44 type truck. The plate was supposed to evenly distribute the applied load over the entire area of plate. The thickness of the plate was changed to three inches after the testing of the five vertical web members in the first test bridge deck panel because a plastic hinge developed in each of the plates at an applied load of 36 kips (see Appendix G). Table 3.2 gives the values for the permanent set for each testing position. As soon as the plastic hinge was developed, the applied load was not being evenly distributed over the footprint of the steel test pad for tests 1 through 5, voiding the purpose of the HS25-44 test pad. At an applied load of 36 kips, the plastic hinge was beginning to be developed in the plates (see Appendix G). To overcome this problem, a three-inch plate was used in testing positions 6a, 6b, and 7, increasing the flexural rigidity by a factor of 27 and the load required to develop the plastic hinge by a factor of 9. The vertical and offset diagonal web members of the composite FRP deck panel were sufficiently strong at AASHTO HS25-44 design load. Even the weakest web member (testing position 4) achieved an ultimate load that was almost twice the design load of 20 kips.

Table 3.2 Permanent Set in Each Testing Plate Due to the Development of Plastic Hinge

Test Number	Measured Permanent Set [inches]
1	0.1615
2	0.3115
3	0.0590
4	0.0210
5	0.0035
6a	None[a]
6b	None[a]
7	None[a]
a – Load required to develop a plastic hinge in the 3-inch thick steel plates was never achieved (see Appendix G)	

The actual and adjusted deflection measurements at the design load of 20 kips of applied load are given in Table 3.3. The actual deflections were the values measured by the DCDT at the corner of the steel test pad. The adjusted deflections were found by extending the line defining the primary linear elastic portion to the deflection axis and adjusting the origin to the point of

intersection with the deflection axis. Looking at Table 3.3, the adjusted deflection for the offset diagonal web members (testing position 6a, 6b, and 7) only varied slightly at the design load. In comparison, there was greater variance in the adjusted deflections of the vertical web members. From Figure 2.9, it can be seen that loading positions 4 and 5 were tested between previously failed webs and over epoxy-bonded joints, thus adversely affecting the ability to compare these deflections with the deflection of testing positions 1, 2, and 3.

Table 3.3 Summary actual and adjusted deflection at design load of 20 kips

Test Number	Actual Deflection[a] [inches]	Adjusted Deflection[b] [inches]
1	0.146	0.067
2	0.081	0.049
3	0.107	0.077
4	0.076	0.090
5	0.120	0.057
6a	0.111	0.061
6b	0.105	0.056
7	0.134	0.047
a – See Appendix B for raw data b – See Appendix D and Section 3.5		

3.3 ULTIMATE LOAD CAPACITY

One of the main goals of the load bearing testing program of the FRP composite panels was to determine the ultimate load capacity of the web members and correlate failure behavior response between adjacent failed members. Because of the varied testing conditions previously mentioned in Sections 3.1 and 3.2, the ultimate load capacities were significantly different, mainly due to the change from the flexible plate to the rigid plate. The stress was excessively high in the portion of the vertical web members (testing positions 1 through 5) at the point of load application, due to the development of the plastic hinge in the steel plate, causing premature failure. From earlier discussions, loading positions 4 and 5 were tested over joints between previously failed web members. It is assumed that the relatively low ultimate strength values can be attributed to the residual effects of the failure of testing positions 1, 2, and 3, and the 20 kip difference in the ultimate strength can be accounted for in the variability in the epoxy bonded joint. For the offset diagonal web members, the applied load was spread out over the entire footprint up to the ultimate load, distributing the stress in the web and flanges more evenly. See Table 3.4 for a summary of ultimate load capacities.

Table 3.4 Summary of Ultimate Load Capacities and Deflections

Test Number	Ultimate Load [kips]	Actual Deflection [inches]	Adjusted Deflection[c] [inches]
1	72.04	0.440	0.361
2	83.02	0.374	0.342
3	74.10	0.416	0.386
4	34.00	0.140	0.153
5	54.06	0.236	0.172
6a	106.40[a]	0.668	0.618
6b	116.16[b]	0.634	0.585
7	138.12	0.695	0.608

a – Testing was stopped prematurely because load frame lifted off reaction floor

b – Same position was retested in fully restrained configuration

c – Accounts for initial nonlinearity adjustment (see Section 3.4.1)

The restraint conditions of the testing had secondary effects on the ultimate load capacity. As reported in Table 3.4, position 6a was only partially restrained, carrying 106 kips of applied load when testing was stopped; position 6b failed at 116 kips. It is difficult to characterize the effect of the restraint conditions on the ultimate load capacity.

The load positions were broken down into three categories: vertical webs (tests 1, 2, and 3), vertical webs over joints (tests 4 and 5), and diagonal webs (tests 6b and 7). Test 6a was not included in this last group because testing was interrupted before the ultimate load capacity was achieved. Table 3.5 provides a summary of the average and standard deviation for each of the categories. The standard deviation for the three categories varied significantly.

Coupon samples were extracted tested from the DuraSpan^{TM} 500 FRP panels. Looking at Table 3.6 for the tensile and compressive coupon tests specimens for 0º (parallel to the direction of pultrusion) and 90º (perpendicular to the direction of pultrusion) directions, there was variance in the failure load, especially in the tensile 90º specimens (test results from Yulismana 2004).

Table 3.5 Averages and Standard Deviations of Ultimate Load Capacities

Category (Number of Samples)	Average Ultimate Load [kips]	Standard Deviation [kips]
Vertical Webs (3)	76.4	5.8 (7.6%)
Vertical Webs Over Joints (2)	44.0	14.2 (32.3%)
Diagonal Webs (2)	127.1	15.5 (12.2%)

Table 3.6 Averages and Standard Deviations of the Failure Load of Coupon Tests

Category (Number of Samples)	Average Failure Load [kips]	Standard Deviation [kips]
Tensile (0º) (5)	24.4	0.33 (2.9%)
Tensile (90º) (5)	11.4	8.40 (33.9%)
Compressive (0º) (4)	35.7	0.85 (3.8%)
Compressive (90º) (5)	22.7	1.5 (4.1%)

3.4 DISCUSSION OF LOAD DEFLECTION RELATIONSHIPS

The behavior of the composite FRP bridge panel under the applied loading conditions should produce a linear elastic stress strain relationship (as well as load deflection relationship) until the point of rupture failure (Scott, Wheeler 2001). By looking at the load deflection curves in the Appendix C, there was double linear elastic curvature for all testing positions except position 4 (see Section 3.4.1). Peculiarities in each test (thickness of testing plate, restraint conditions, and the placement of the DCDT) affected the true measurement of the deflection at a given applied load. Though all tests were not conducted under the same conditions, useful (and adjusted) deflection data can be extracted from the measured data. Each of the load deflection curves will be divided into three parts:

1. Initial anomalies,
2. Primary linear elastic region including the transition zone, and
3. Secondary linear elastic region.

Each of the following will be analyzed and explained, and finally the load deflection curves will be adjusted to reflect assumptions about the actual data collected under the given testing conditions.

3.4.1 Initial Anomalies

There are two justifications for eliminating the initial anomalies. In Section 1.3, the make up of the FRP panels was discussed. The nexus is a thin layer that is added to the surface of the resin

and fibers after leaving the resin bath as shown in Figure 1.2. The Modulus of Elasticity associated with the nexus is almost negligible. This layer does not influence the overall capacity of the web and flanges. Except for position 4 and 7 the load deflection curves were nonlinear during the application of approximately the first 10 kips of load. Test positions 4 and 7 had unique initial nonlinear regions. For position 4, the initial deflection measurements were negative and nonlinear for the first 3 kips of applied load. The initial nonlinear region of position 7 was similar in shape to the majority of testing positions, though the range of nonlinear behavior spanned between the start of loading and approximately 20 kips of applied load.

Another idiosyncrasy with the initial testing conditions dealt with the steel test pads and surfaces of the FRP decks. The plates and the surface profiles of the FRP deck panel were assumed to be perfectly flat, though highly unlikely. Unless the surface profile of the top of the FRP deck section was exactly the same as the surface profile as the underside of the steel testing plate, initial increments of applied loading was settling the plate and FRP panel to be in complete contact with the each other as well as compressing the outer layers (nexus) of FRP in contact with the steel plate and reaction floor. The initial nonlinear portions of the load deflection curves will be ignored, and adjusted curves will be created to reflect these corrections. The adjusted deflections are found by extending the line defining the primary linear elastic portion to the deflection axis (horizontal axis) and adjusting the origin to the point of intersection with the deflection axis (see Figure D 1). Given in Table 3.7 was the change in the location of the origin with respect to the corrections for the initial nonlinear behavior.

Table 3.7 Corrections For Deflections Due to Initial Nonlinearities

Test Number	Correction of Deflection [a] [inches]
1	0.0786
2	0.0320
3	0.0302
4	-0.0136[b]
5	0.0720
6a	0.0505
6b	0.0489
7	0.0870
A – Corrections for initial nonlinearities B – Negative due to testing anomaly	

3.4.2 Primary Linear Elastic Region and Transition Zone

With compressive loading, the load deflection curves should be linear elastic until the point of failure. The curves from the compressive coupon tests (given in Yulismana 2004) show that the behavior prior to failure produced a linear elastic stress strain relationship. After the initial loading anomalies, the web and flanges of the FRP deck section were supporting the applied load. The primary linear elastic portion of the curve was being formed. At an applied load of 42 kips, all the testing positions except 4 and 7 exhibited nonlinear behavior, until the slope gradient decreased to a constant value consistent with the slopes of the secondary linear elastic regions. Testing position 4 never achieved an applied load of 42 kips nor did it have a nonlinear transition zone; testing position 7 was loaded under fully restrained testing conditions such that its nonlinear transition zone began to form at a higher applied load. The points of tangency and the intersection of the two linear elastic portions are shown in Table 3.8 (also see Figure 3.1). The lower point of tangency denotes the last load in the primary linear elastic region; the upper point of tangency was the first load in the secondary linear elastic region (see section 3.4.3). The intersection is the point where the tangent lines cross. In position 4, there were no points of tangency, due to premature failure. The testing conditions of position 7 dictate the higher load values for the points of tangency and intersection.

Table 3.8 Points of Tangency and Intersection of Linear Elastic Regions

Test Number	Lower Point of Tangency [kips]	Intersection of Tangents [kips]	Upper Point of Tangency [kips]
1	42	47	54
2	42	46	52
3	42	46	48
4	NA[a]	NA[a]	NA[a]
5	42	43	46
6a	42	48	54
6b	44	45	48
7	52	54	56

a – Testing position failed prematurely

3.4.3 Secondary Linear Elastic Region

The secondary linear elastic region of the load deflection curves formed at a range of applied loads between 46 kips and 56 kips (except loading position 4), which are consistent with the upper points of tangency given in Table 3.8. It is possible that the existence of the secondary linear elastic region could be attributed to the inaccurate measurements of the deflections. It is equally possible that architecture of the fiber orientation with respect to the respect the direction of loading of the FRP web and flanges dictates the decrease in stiffness as compared to the stiffness of the primary linear elastic region. A more in depth explanation of the secondary linear elastic region phenomena is discussed in Section 4.2.

3.5 ADJUSTMENTS OF CURVES

In Appendix D, the load deflection curves are shown with the adjusted deflection readings due to the initial loading anomalies. As explained in Section 3.2, the initial nonlinear deflection anomalies were removed by extending a line defining the primary linear elastic region of the curve to the deflection axis and adjusting the origin to the intersection. The adjustment value, given in Table 3.7, was subtracted from every deflection measurement (see Appendix B for original data) for each respective testing position. All points defining the initial nonlinear deflections were removed, leaving only a point at the adjusted origin, the adjusted data defining primary linear elastic region of the curve and the data points thereafter (see Figure D 1).

Because of the elastic nature of the composite FRP bridge deck panel and the location of the DCDT, the measured deflections were inaccurate for the flexible steel test pads (positions 1 through 5). The true deflection of the steel test pad was at the center of the plate. Using Hetényi's beam on elastic foundation model (see Appendix F) and the measured deflection at the end of the plate at the applied load defining the last point of the linear elastic region of load deflection curves (i.e. lower point of tangency, see Table 3.7 and Figure 3.1), the true deflection at the center for that load was calculated. In Hetényi's model the only unknown in Equation F 2 was the modulus of the foundation (i.e. the FRP deck), and from Equation F 1 the deflection at the center of the plate could be calculated. The points defining the primary linear elastic region of the curves were replaced by a straight line between the adjusted origin and a new point, at the load at which the lower point of tangency and its corresponding deflection were calculated at the center of the plate from Hetényi's model. The difference between the deflection at the center of the plate and the actual deflection measured by the DCDT was added to all remaining points defining the transition zone and secondary linear elastic region (see Figure D 2).

The data obtained from the testing sequence of the flexible plates cannot be directly compared to the data tests using the rigid plates. The ideal condition for testing would have been to use the rigid plates for all tests. Using Hetényi's beam on elastic foundation model, the deflections at the center of the plate that would have resulted had a rigid plate been used (see Figure D 3).

Since it was speculated that the development of the plastic hinge only contributed to the stress concentrations in the web beneath the application of the load and not to the inaccurate deflection measurements (see section 4.2), the measured permanent set given in Table 3.2 for steel testing pads 1 through 5 will not be added to the final deflection at the ultimate load. For

consistency all points, except for the point of the adjusted intersection of tangent lines to the primary and secondary linear elastic regions and the deflection at the ultimate load, have been deleted; leaving a curve only defined by four points unless the point of intersection is approximately the same as the lower point of tangency or if the test terminated before the application of loads great enough to cause a secondary linear elastic region.

3.6 DISCUSSION OF STRESS STRAIN RELATIONSHIPS

The adjusted load deflection relationship described in Section 3.5 was transformed to reflect an equivalent stress strain relationship. From the adjusted load deflection curves, stress strain curves were derived. Although deflections measured with a DCDT were not as precise as those with a strain gauge, nominal stresses and strains can be calculated. To convert load into stress, the measured load values were divided by the area of bearing. The bearing area was the length of the steel plate (20 inches) multiplied by the nominal thickness of the web (0.25 inches). The adjusted deflection values were converted to strain by dividing the deflection by the nominal depth of the web (3.75 inches). See Appendix E for the unadjusted and adjusted stress strain curves for each testing position.

3.7 FAILURE MODES

It was important to have an understanding of how each of the FRP web and flanges failed upon achieving ultimate load capacity. The governing factor in the failure of the webs rests in the thickness of the steel test pads. At the development of the plastic hinge in the flexible steel testing pads (testing positions 1 through 5), the applied load was being concentrated at the center of the plate in the direction of traffic. Due to the concentrated line load, the maximum stress concentration in the web and flanges was directly beneath the application point of load application. For test positions 6a, 6b, and 7, a three-inch thick rigid plate was used. The applied load was spread evenly over the surface of the plate, and the stress was uniformly developed in the section of the web and flanges directly beneath the footprint of the steel test pad.

The exact determination of the failure mechanism of the FRP web and flanges is impossible due to the loading conditions, though speculations can be made with respect to the testing conditions and the data collected. The testing occurred in load-controlled mode instead of deflection-controlled mode. In load-controlled mode loading continued after the specimens failed and the pump was turned off, consequently subjecting the failed location of the FRP panel to additional loading. The additional few seconds of loading caused further damage to the decks, especially at test positions 6b and 7, creating difficulty in determining the true failure mode of each loading position, as well as additional permanent deformation to the steel test pads for loading positions 1 through 5.

For test positions 1 through 5, there was some minimal delamination of the outer face sheets of the web, in addition to a stress fracture line in the web that extended slightly beyond the

footprint of the steel test plate and that was greatest directly under the point of load application. There was no noticeable damage to the top flanges of the FRP deck panel. For testing positions 6b and 7, there was complete crushing of the web in the area beneath the footprint of the steel test pad as well as punching shear failure of the top flange around the footprint of the steel test pad.

4.0 DISCUSSION AND CONCLUSIONS

4.1 INTRODUCTION

In the previous chapter, the load deflection curves were adjusted to reflect the true reading of the deflections at the center of the steel test pad and for the hypothetical situation where the flexible test pads for testing positions 1 through 5 were replaced with rigid test pads. The hypothetical modeling enabled comparison between all testing positions that was not feasible when using the unadjusted, measured data. Though the adjustments to the load versus deflection curves have been performed, the adjusted data left one question unanswered. If the coupon specimens tested in compression by Yulismana exhibit linear elastic behavior until failure, why do the load deflection curves for the bearing capacity test specimens have two linear elastic regions with different slopes, instead of a single linear elastic region until failure? The answer is neither simple nor cut and dry. Several major causes that will be considered in the following section will either prove or disprove the assumptions presented. Finally, conclusions will be drawn with relation to the discussions presented in Section 3.5 and Section 4.2 as well as the purpose of the testing program.

4.2 FINAL DISCUSSION OF LOAD DEFLECTION RELATIONSHIPS

To grasp an understanding of the behavior of FRP under the testing conditions, identification of possible causes was necessary to explain the existence of the two linear elastic regions, instead of a single linear elastic curve until failure. The possible causes explored in this thesis are:

1) The mechanism securing the entire composite FRP panel to the reaction floor,
2) The failure and delamination of an outer layer or face sheet of lamina in the web under the applied loading,
3) The thickness of the steel test pad and subsequently the development of the plastic hinge, and
4) The flexibility in the tube steel restraints and in the bolted connections attaching the crossbeam to the columns and the columns to the main beams.

As mentioned in Section 2.5, the mechanisms securing the FRP deck on two opposite sides were oriented parallel to the direction of traffic (perpendicular to the direction of pultrusion, see Figure 2.7). Due to the makeup of the cross section of the panels and the lack of restraint in the direction perpendicular to traffic, it is possible that the top flange of the panel shifted with respect to the bottom flange, creating an eccentric loading condition and subsequently a small P-δ moment. Due to lack of visual evidence during and after testing and the lack of ability to quantify the effect of the P-δ moment with respect to double linear elastic behavior of the load deflection relationships, mechanism securing FRP panel to reaction floor will be dismissed as a probable cause.

The possibility that the existence of two independent linear elastic ranges in the load deflection curves is related to the delamination in the web of the FRP deck panel can be refuted by examining the data from tests 6a and 6b. It is assumed that the load deflection curve became nonlinear at the initiation of failure of an outer face sheet, and then returned to a linear elastic curve once the outer lamina was completely delaminated. After delamination completely occurred, the stiffness of the web decreased, corresponding with the change in slope of the load deflection curve. Test position 6a (partially restrained) was loaded until it was realized that the load frame began to lift off the reaction floor; testing was stopped immediately and prior to ultimate failure. If the transition zone between the two linear elastic portions was caused by the initiation of failure and ultimately delamination of an outer lamina, the stiffness of the secondary linear elastic region in testing position 6a should be equal to the stiffness of the primary linear elastic region in testing position 6b. By examination of the curves, the stiffness of primary linear elastic region of test 6b is very similar to the stiffness of the primary linear elastic region of test 6a (see Figure 4.1). This proves that there was no initiation of yielding (or failure) and delamination at the start or through the completion of the transition zone. In addition, the primary linear elastic region of testing position 6b is slightly stiffer that that of testing position 6a. It is possible that the web was strain hardened during the first loading sequence, though it is more likely that it was an idiosyncrasy coupled to the change from the partially restrained conditions of test 6a to the fully restrained conditions of test 6b (see Figure 4.1 for a comparison of unadjusted curves for 6a and 6b).

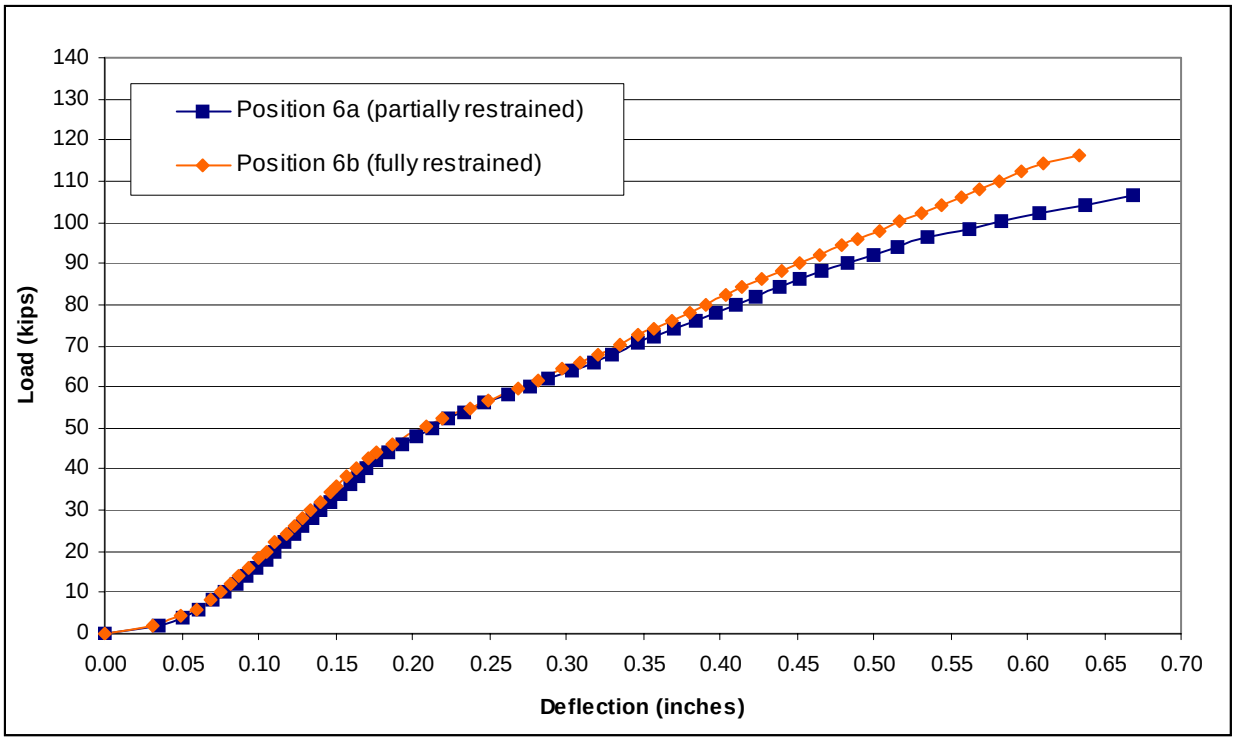

Figure 4.1 Comparison of Testing Positions 6a and 6b

There was significant visible permanent deformation in all of the flexible steel test pads (see Table 3.2). From examination of the unadjusted load deflection curves for testing positions 1 through 5, the development of the plastic hinge in the steel test pads appears to be a reasonable explanation for the double linear elastic curve geometry. Assuming the steel test pad was made from 36 ksi steel, the development of the plastic hinge occurred around 36 kips of applied load, possibly affecting the measured deflections, though the load at which the initiation of the plastic hinge formed, varied depending on the yield stress of the steel test pad (see Appendix G). The yield strength of steel test pads is unknown because coupon specimens were not tested to verify the mechanical properties. If the theory of the development of the plastic hinge in the flexible steel plate were to hold true for the rigid steel plates, the load versus deflection relationships should be linear elastic for tests 6a, 6b, and 7 until approximately 324 kips of applied load; a load

that would never be achieved because the actuator has a maximum capacity of 200 kips. As shown in Table 3.7 and the load deflection curves for testing positions 6a, 6b, and 7, the transition zone began to form at applied loads of 42, 44, and 52 kips, respectively. It can be concluded that the development of the plastic hinge in the steel plates did not adversely affect the measured deflections, though it affected the ability to evenly distribute the applied load over the footprint of the steel test pad, consequently affecting the ultimate strength.

Since three of the possible causes that will be explored in this thesis have been ruled out, only one cause remains, the flexibility in the restraints as well as in the components of the load frame. If the load frame had been secured on both sides of the point of load application (see Figure A 2), and the load frame, connections in the load frame, steel test pad, and all components making up the tie-down supports (i.e. HSS8x8, threaded rods, bolts, etc.) were perfectly rigid, the load deflection relationship would behave in a linear elastically until failure. Since attaining perfectly rigid conditions is nearly impossible, it is to be expected that there would be some flexibility in the load frame and tie-down restraints. Again, positions 6a and 6b provide the most significant insight into this phenomenon. In Figure 4.1, the load deflection relationship for the unadjusted data for positions 6a (partially restrained) and 6b (fully restrained) is provided. Since both sets of data had similar deflections for a given applied, primary stiffnesses, and transition zone regions, it can be concluded that the restraint conditions were not the cause of the secondary linear elastic region.

Even though the restraint conditions were not the cause of the two linear elastic regions, the partially restrained conditions did affect the accurate measurement of the deflection when the load frame began to lift off the reaction floor. Liftoff was not noticed until approximate 106 kips of applied load. By inspection of the curves in Figure 4.1, the curve for position 6a began to

deviate from linear elastic behavior at approximately 96 kips of applied load, whereas position 6b continued in a linear elastic foundation until failure.

All of the assumptions presented in this section to explain the possible causes for the two linear elastic regions have been disproved through the examination of the data collected from testing positions 6a and 6b.

4.3 CONCLUSIONS

One of the purposes of the bearing testing program was to determine if the FRP deck panel was sufficiently stiff to withstand HS25-44 type loading when tested directly over the vertical and offset diagonal webs. The data presented in Chapter 3 validates the assumption that the FRP panels were sufficiently strong to support AASHTO design loads. The vertical web, that failed prematurely (testing position 4) and had the lowest calculated modulus of elasticity from the unadjusted stress versus strain curves, was loaded to almost twice the required design load of 20 kips. As shown on adjusted load deflection curves presented in Appendix D and the data given in Table 4.1, the deflection at the design load is useful to code writing bodies and designers. The secondary purpose of the bearing capacity tests was to determine the ultimate load capacity and corresponding deflection for each testing position (see Table 4.2). The deflections at the ultimate load for testing positions 6a, 6b and 7 were about one-tenth of the nominal depth of the FRP composite bridge deck panel. At the design load, the deflections are less than one-tenth of an inch.

Since all of the raw data collected from the series of eight bearing tests (seven testing positions) was not directly comparable, modifications and adjustments were made to remove initial nonlinearities and to reflect a hypothetical situation in which all tests were performed with rigid steel test pads. In addition, additional testing of coupon samples and deck panels are necessary to verify the coexistence of the cause(s) for the linear elastic regions. From Figure D 3, a better understanding of the true behavior of the FRP deck under the given AASHTO HS25-44 loading conditions can be understood and ultimately compared to future studies of the bearing capacity.

Table 4.1 Adjusted Deflection Values At the Design Load Capacity of 20 Kips

Test Number	Deflection at Design Load[a] [inches]
1	0.078
2	0.051
3	0.081
4	0.098
5	0.056
6a	0.062
6b	0.060
7	0.073
a – From adjusted data in Appendix D	

Table 4.2 Adjusted Deflection Values At the Ultimate Load Capacity

Test Number	Ultimate Load [kips]	Deflection At Ultimate Load[a] [inches]
1	72.04	0.381
2	83.02	0.346
3	74.10	0.390
4	34.00	0.157
5	54.06	0.171
6a	106.40	0.622
6b	116.16	0.589
7	138.12	0.612
A – From adjusted data in Appendix D		

5.0 RECOMMENDATIONS

The difficulties that were faced during the testing could have been circumvented if the schedule for the completion of the tests had not been so rigorous, and if analysis and evaluation were performed after the completion of testing at each position. Further testing under fully restrained conditions with a rigid steel test pad should be completed to verify the results and assumptions provided in this thesis. The procedure for future testing should incorporate the determination of the ultimate load capacity. Because of the linear elastic, non-yielding nature of FRP, all of the desired testing positions should be tested close to failure (a predetermined load of 100 kips), and then each position should be retested to determine the ultimate load capacity. Coupon specimens should be extracted from each of the webs at each testing position to verify material properties. In addition, a small section of web with adjacent flanges should be removed and tested under compressive loading, to help begin understanding the true failure modes of the web

If the architecture of the cross section of the FRP panel were solely based upon the design with accordance to the bearing capacity of the vertical and offset diagonal web members, the thickness and/or the constituents of the web members could be altered. Because the ultimate load capacity was almost twice as large as the AASHTO HS25-44 specifications, some fiber reinforcement could be removed from the web without compromising the design load capacity. The constituents of the web are assumed to be E-glass fibers and polyester resin. The quantity and type of fiber reinforcement drives the cost of FRP. If the amount of fiber reinforcement

were reduced for the specific design application, FRP bridge deck panels would become a more attractive and cost effective alternative to conventional steel reinforced concrete bridge decks.

APPENDIX A

LOAD FRAME

Drawings detailing the setup of the load frame at the time of testing and the free body diagrams for partially and fully restrained testing conditions are presented within this Appendix. In Figures A 1 and A 2, it should be noted that the DuraSpan^{TM} 500 FRP panels for the bearing test are not shown. Testing of the panels occurred in the area between the diaphragms beneath the leftmost column.

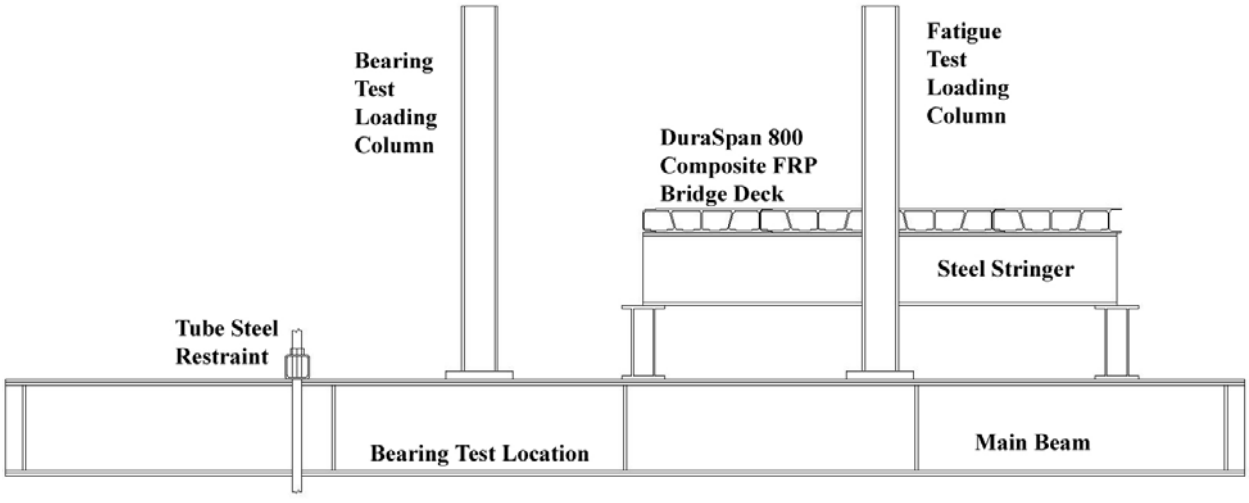

Figure A 1 Partially Restrained Load Frame At the Time of Testing

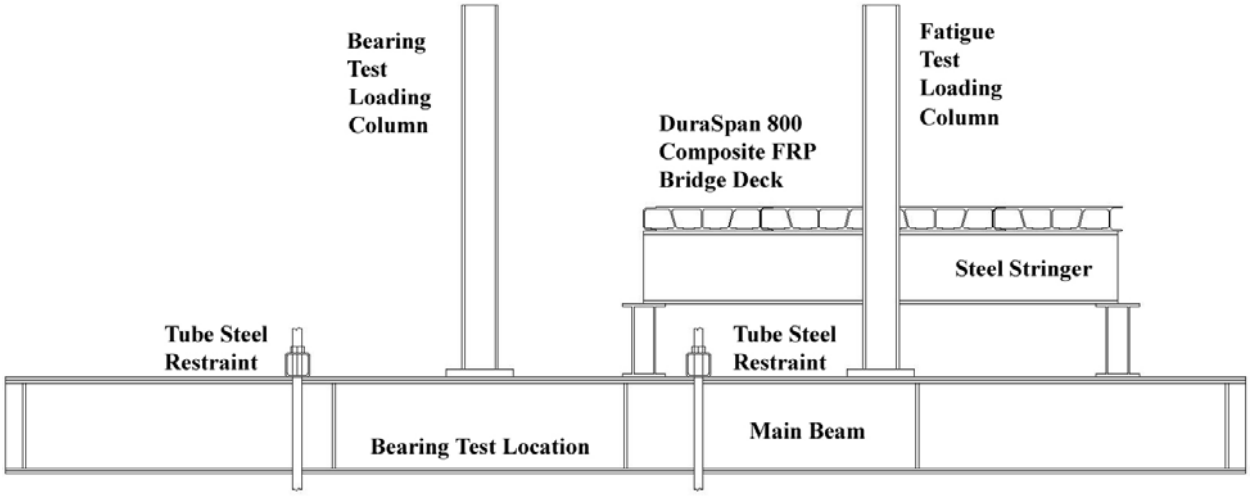

Figure A 2 Fully Restrained Load Frame At Time of Testing

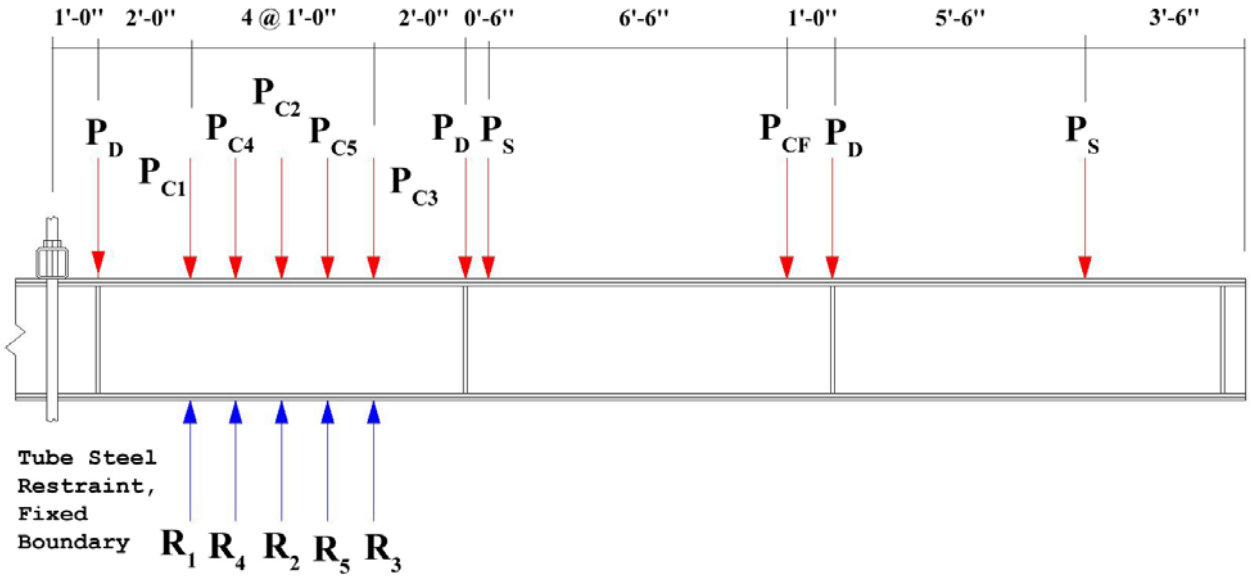

Figure A 3 Free Body Diagram of Partially Restrained Load Frame At the Time of Testing

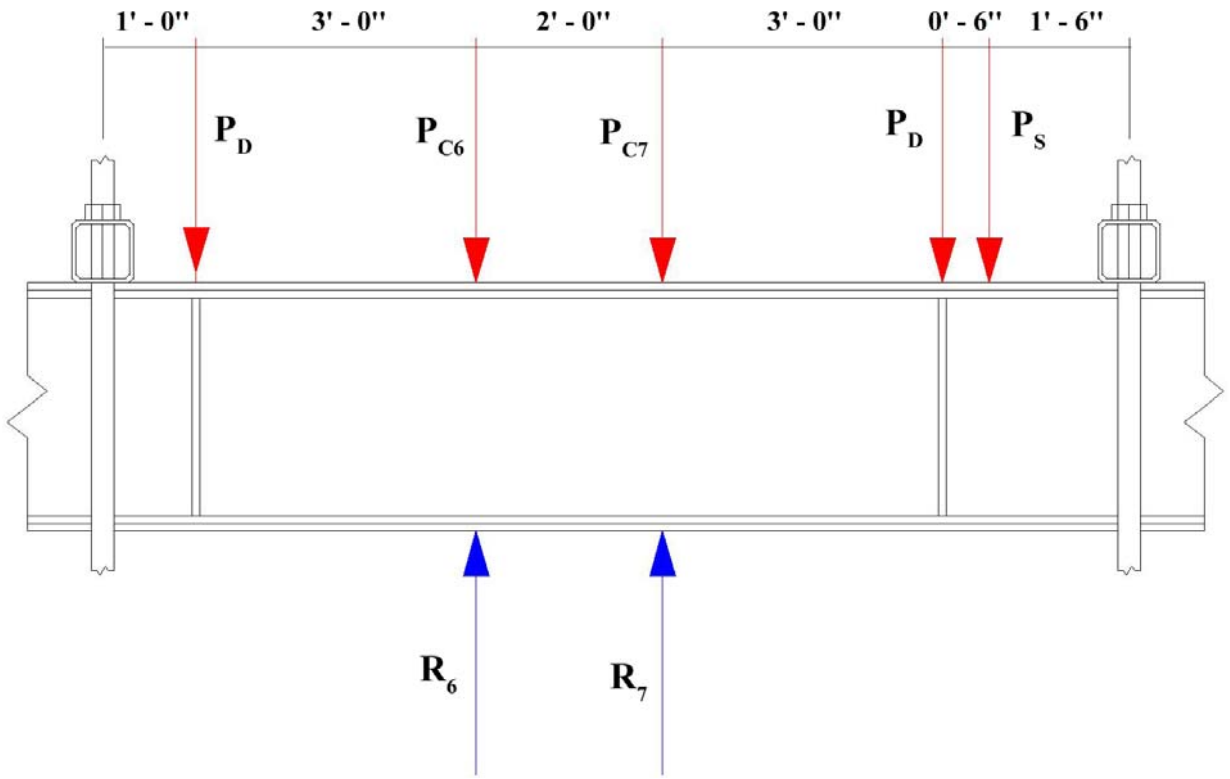

Figure A 4 Free Body Diagram of Fully Restrained Load Frame At Time of Testing

In Figures A 1 and A 2, the position of the bearing test loading column changed with respect to the FRP composite web being tested. In Figures A 3 and A 4, only one reaction and numbered column load would be used in a numerical analysis. The two restraints in Figure A 4 fully fix the boundaries at their respective locations; any external dead load applied outside of the bounds of the restraints do not affect numerical analysis. The following is the descriptors for each variable for the free body diagrams:

$R_X \equiv$ Uplift reaction due to applied load at each position

$P_{CX} \equiv$ Dead load of column system for bearing test at each load position

$P_D \equiv$ Dead load due to diaphragms

$P_{CF} \equiv$ Dead load of column system for fatigue test

$P_S \equiv$ Dead load of reaction support and half of DuraSpan^{TM} 800 deck

$X \equiv$ Test number associated with column position.

Two external forces not shown in either free body diagram diagrams are:

1) Self weight of the main beam, W_B, and
2) Normal force from the reaction floor.

The approximate values for the components listed above and shown in the free body diagrams are:

$P_{CX} = 8{,}750$ lbs

$P_D = 1{,}025$ lbs

$P_{CF} = 8{,}750$ lbs

$P_S = 3{,}900$ lbs

$W_B = 264$ lbs / ft

Figure A 5 Overview of Load Frame After the End of Testing

Figure A 6 Connection Detail of Loading Column and Crossbeam

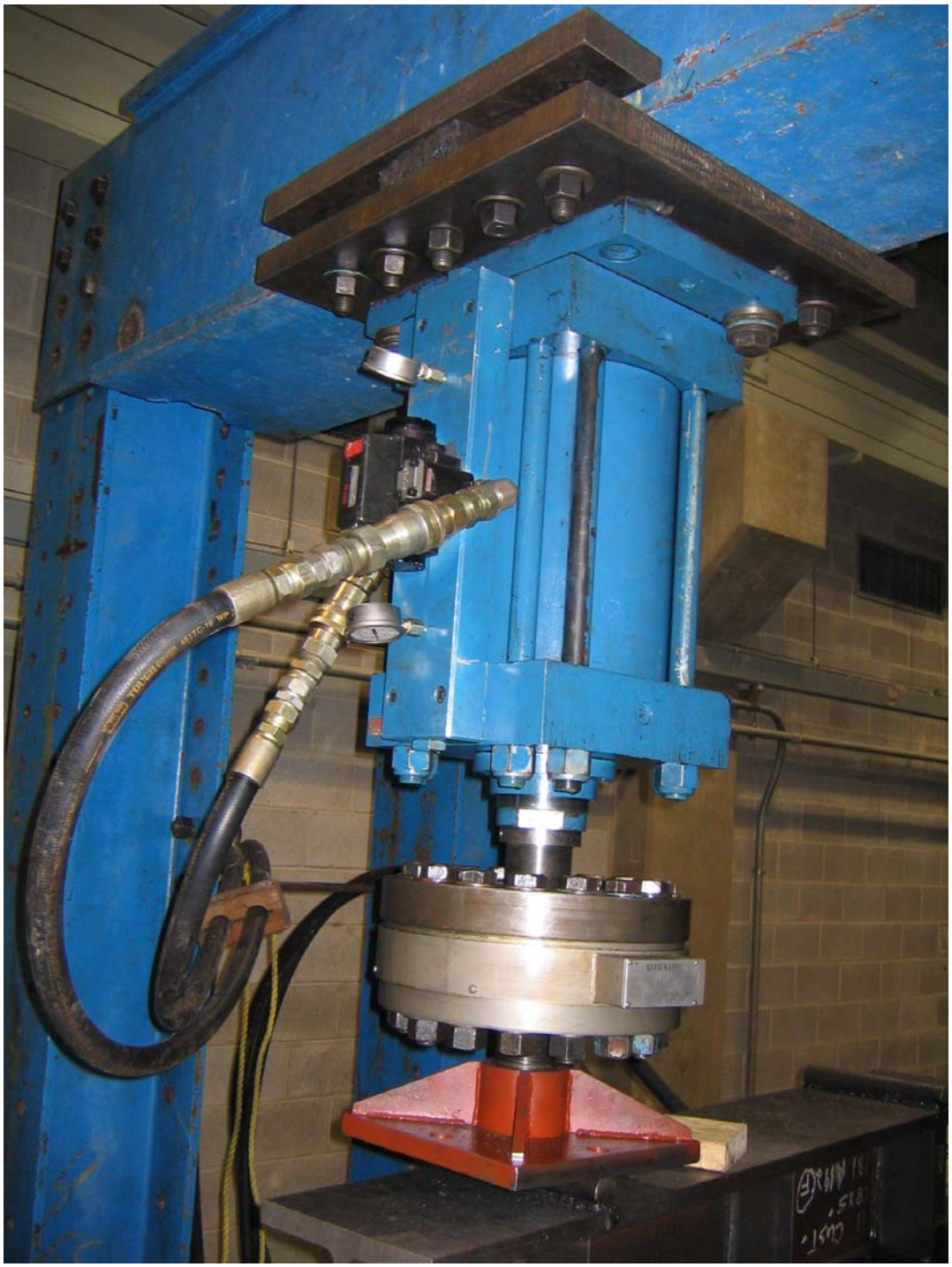

Figure A 7 Connection Detail of Actuator to Crossbeam

Figure A 8 Connection Detail of Tube Steel Restraint

Figure A 9 Representative Layout of DCDT Placement on HS25-44 Steel Test Plate

Figure A 10 Data Acquisition System

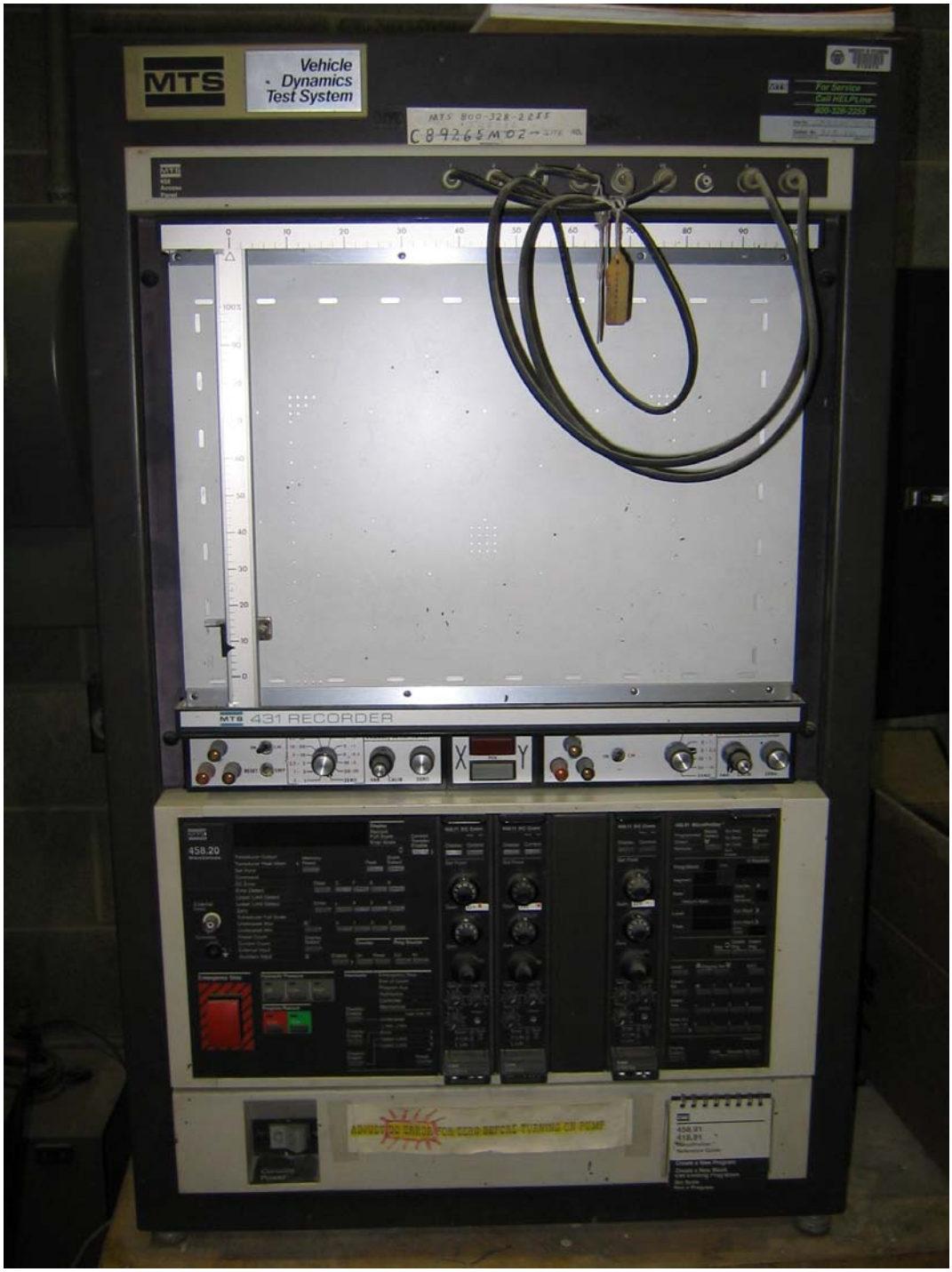

Figure A 11 MTS 458 With a Micro-profiler

APPENDIX B

RAW DATA COLLECTED FROM EACH TESTING POSITION

Table B 1 Raw Data From Testing Position 1

Load [kips]	Deflection [inches]	Load [kips]	Deflection [inches]
0.00	0.00000	30.02	0.18218
1.04	0.04131	32.02	0.18855
1.98	0.05524	34.06	0.19571
3.04	0.06320	35.96	0.20208
4.06	0.07155	38.04	0.20884
5.14	0.07862	40.04	0.21521
6.12	0.08588	42.10	0.22237
7.00	0.09085	44.04	0.23232
7.98	0.09822	45.04	0.23829
9.02	0.10418	46.12	0.24426
9.96	0.10856	48.12	0.25500
11.08	0.11334	50.14	0.26574
12.02	0.11771	52.06	0.27689
12.96	0.12169	54.20	0.29121
14.00	0.12567	55.10	0.29877
15.02	0.12965	56.06	0.30673
16.08	0.13323	57.14	0.31549
17.00	0.13742	58.38	0.32583
18.14	0.14019	60.00	0.33976
19.06	0.14395	61.02	0.34772
20.34	0.14836	63.04	0.36443
21.06	0.15154	65.14	0.38154
22.12	0.15572	67.02	0.39746
23.02	0.15791	69.10	0.41497
24.30	0.16248	70.00	0.42333
26.04	0.16865	72.04	0.43982
28.04	0.17581		

Table B 2 Raw Data From Testing Position 2

Load [kips]	Deflection [inches]	Load [kips]	Deflection [inches]
0.00	0.00000	50.00	0.17191
1.94	0.01313	52.30	0.18225
4.06	0.03104	54.08	0.19061
6.00	0.04178	56.12	0.20175
7.98	0.04934	58.14	0.21528
10.02	0.05571	60.12	0.22762
12.02	0.06088	62.00	0.23955
14.02	0.06606	64.24	0.25348
15.98	0.07083	66.10	0.26502
18.02	0.07600	68.08	0.27696
19.96	0.08078	70.04	0.28890
22.06	0.08595	71.00	0.29447
24.04	0.09113	72.12	0.30123
26.06	0.09590	73.04	0.30680
28.06	0.10068	74.06	0.31317
30.00	0.10585	75.00	0.31874
32.04	0.11102	76.02	0.32551
34.08	0.11580	77.04	0.33227
36.08	0.12057	78.10	0.33904
38.02	0.12495	79.30	0.34700
40.00	0.13012	80.04	0.35257
42.00	0.13450	81.14	0.36013
44.04	0.14246	82.12	0.36689
46.00	0.15320	83.02	0.37366
48.08	0.16315		

Table B 3 Raw Data From Testing Position 3

Load [kips]	Deflection [inches]	Load [kips]	Deflection [inches]
0.00	0.00000	38.12	0.18085
3.06	0.03023	40.00	0.18862
5.14	0.04476	42.16	0.19637
7.12	0.05391	44.06	0.20632
9.16	0.06386	46.02	0.21826
11.00	0.07182	48.08	0.22980
13.06	0.07978	50.06	0.24293
15.12	0.08893	52.00	0.26004
17.00	0.09649	54.00	0.27715
19.16	0.10525	56.06	0.29347
21.38	0.11440	58.12	0.31058
23.12	0.12156	60.06	0.32610
24.94	0.12912	62.24	0.34221
27.10	0.13728	64.38	0.35953
30.18	0.15061	66.14	0.37226
32.08	0.15817	68.20	0.38738
34.00	0.16573	70.32	0.40250
36.00	0.17290	72.16	0.41603

Table B 4 Raw Data From Testing Position 4

Load [kips]	Deflection [inches]	Load [kips]	Deflection [inches]
0.00	0.00000	18.17	0.06844
2.32	-0.00756	20.02	0.07640
5.08	0.01034	22.04	0.08555
8.08	0.02507	24.08	0.09670
10.04	0.03422	26.00	0.10664
12.00	0.04258	28.06	0.11818
14.08	0.05233	30.04	0.12972
16.04	0.05969	32.00	0.13967

Table B 5 Raw Data From Testing Position 5

Load [kips]	Deflection [inches]	Load [kips]	Deflection [inches]
0.00	0.00000	30.02	0.14883
4.00	0.06367	32.10	0.15440
6.06	0.07521	34.08	0.15997
7.98	0.08317	36.00	0.16554
10.08	0.08993	38.02	0.17111
12.20	0.09710	40.14	0.17668
14.04	0.10227	42.02	0.18186
16.04	0.10824	44.10	0.19082
18.14	0.11421	46.04	0.19976
20.00	0.12018	48.06	0.20812
22.02	0.12654	50.12	0.21767
24.04	0.13291	52.04	0.22623
26.00	0.13848	54.06	0.23598
28.46	0.14485		

Table B 6 Raw Data From Testing Position 6a

Load [kips]	Deflection [inches]	Load [kips]	Deflection [inches]
0.00	0.00000	54.00	0.23359
2.06	0.03502	56.00	0.24712
3.98	0.05054	58.08	0.26184
6.04	0.06168	60.14	0.27617
8.10	0.07044	62.04	0.28870
10.02	0.07800	64.04	0.30362
12.06	0.08516	66.12	0.31755
14.02	0.09232	68.06	0.33038
16.10	0.09829	70.66	0.34740
18.08	0.10466	72.08	0.35734
20.02	0.11102	74.04	0.37048
22.14	0.11739	76.26	0.38440
24.12	0.12336	78.10	0.39754
26.12	0.12893	80.06	0.40987
28.04	0.13490	82.00	0.42300
29.96	0.14047	84.24	0.43892
31.98	0.14684	86.04	0.45245
34.10	0.15321	88.02	0.46657
36.10	0.15957	90.00	0.48269
38.08	0.16435	92.00	0.49941
40.12	0.17071	94.10	0.51552
42.24	0.17708	96.28	0.53522
44.22	0.18504	98.42	0.56188
46.06	0.19379	100.04	0.58257
48.00	0.20274	102.10	0.60744
50.04	0.21329	104.20	0.63828
52.08	0.22324	106.40	0.66831

Table B 7 Raw Data From Testing Position 6b

Load [kips]	Deflection [inches]	Load [kips]	Deflection [inches]
0.00	0.00000	61.60	0.28134
2.10	0.03104	64.28	0.29805
4.22	0.04894	66.12	0.30959
6.02	0.05969	68.02	0.32073
8.28	0.06844	70.38	0.33466
10.10	0.07521	72.44	0.34699
12.14	0.08157	74.16	0.35734
14.02	0.08714	76.10	0.36848
15.98	0.09311	78.16	0.38042
18.46	0.10028	80.08	0.39116
19.98	0.10505	82.18	0.40350
22.06	0.11102	84.06	0.41364
24.08	0.11759	86.28	0.42775
26.00	0.12356	88.22	0.43971
28.14	0.12853	90.00	0.45165
30.02	0.13410	92.06	0.46478
32.04	0.13967	94.30	0.47871
34.36	0.14683	96.00	0.49025
35.92	0.15121	98.04	0.50378
38.04	0.15698	100.10	0.51731
40.14	0.16355	102.08	0.53124
42.46	0.17131	104.04	0.54357
44.18	0.17668	106.26	0.55670
46.18	0.18682	108.10	0.56864
50.50	0.20971	110.10	0.58177
52.14	0.21886	112.16	0.59570
54.82	0.23716	114.18	0.61082
56.78	0.2499	116.16	0.6336
59.74	0.2688		

Table B 8 Raw Data From Testing Position 7

Load [kips]	Deflection [inches]	Load [kips]	Deflection [inches]
0.00	0.00000	72.08	0.37088
5.04	0.00319	74.00	0.38042
7.00	0.02149	76.10	0.39117
10.10	0.04914	78.18	0.40131
12.14	0.06785	80.02	0.41146
14.14	0.08695	82.16	0.42181
16.16	0.10506	84.12	0.43176
18.14	0.12058	86.24	0.44131
20.02	0.13371	88.22	0.45086
22.04	0.14724	90.20	0.46081
24.14	0.16077	92.42	0.47076
26.08	0.16992	94.12	0.47951
28.18	0.18027	96.04	0.48906
30.18	0.18802	98.14	0.49901
32.22	0.19778	100.04	0.50816
34.00	0.20573	102.06	0.51811
36.04	0.21369	104.00	0.52766
38.24	0.22185	106.00	0.53681
40.02	0.22881	108.10	0.54676
42.00	0.23598	110.00	0.55631
44.06	0.24354	112.02	0.56586
46.16	0.25110	114.08	0.57541
48.14	0.25786	116.02	0.58417
50.14	0.26542	118.12	0.59451
52.12	0.27298	120.18	0.60446
54.08	0.28134	122.04	0.61361
56.16	0.29089	124.08	0.62296
58.2	0.30004	126.04	0.63351
60.22	0.3092	128.02	0.64346
62.28	0.31795	130.02	0.65301
64.14	0.32671	132.00	0.66256
66.00	0.33745	134.20	0.67370
68.04	0.34859	136.14	0.68405
70.06	0.35894	138.12	0.69479

APPENDIX C

UNADJUSTED LOAD DEFLECTION CURVES

The individual load deflection curves are presented for the unadjusted data. Figure C 9 is a plot of each of the eight loading positions on one set of axes.

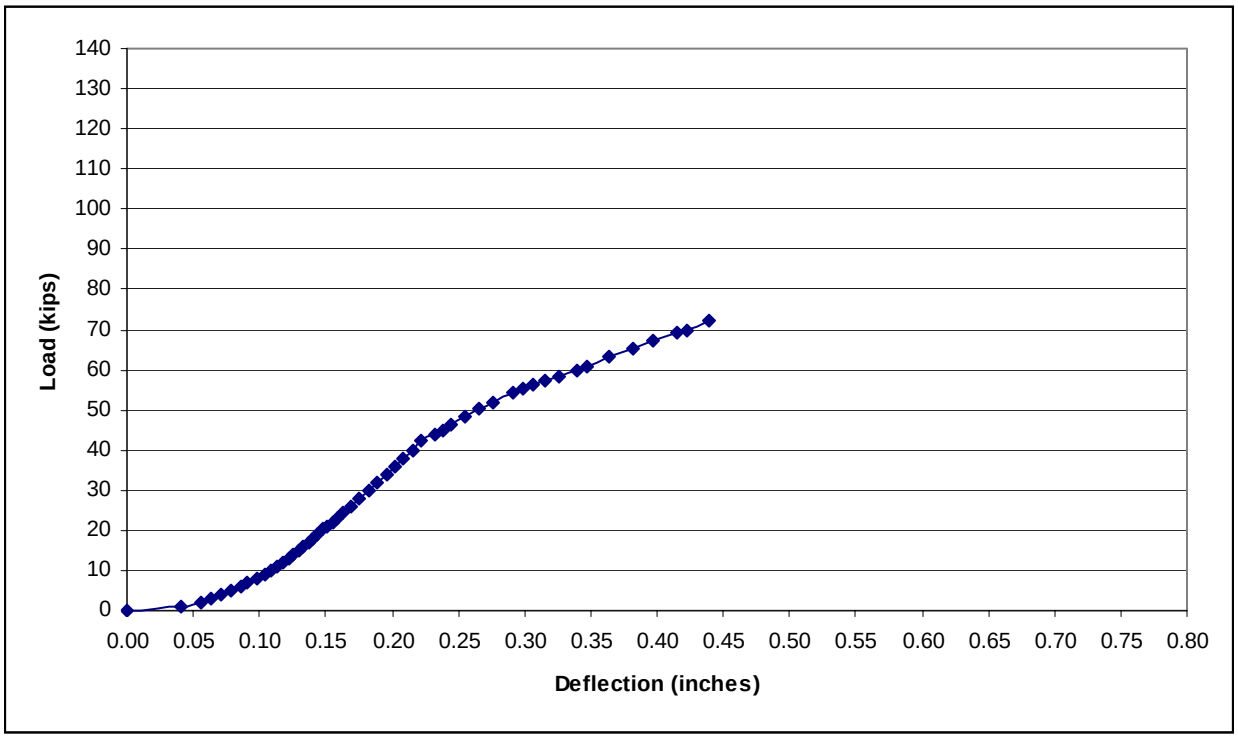

Figure C 1 Unadjusted Load Deflection Curve, Position 1

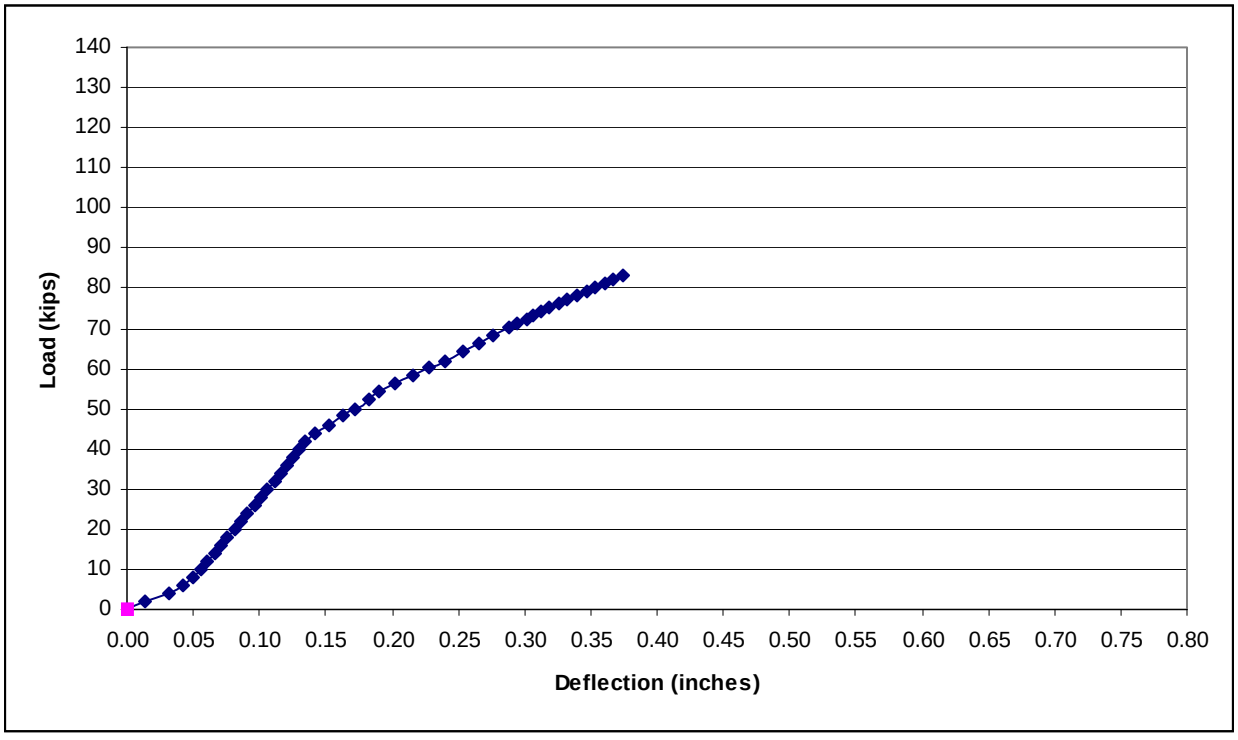

Figure C 2 Unadjusted Load Deflection Curve, Position 2

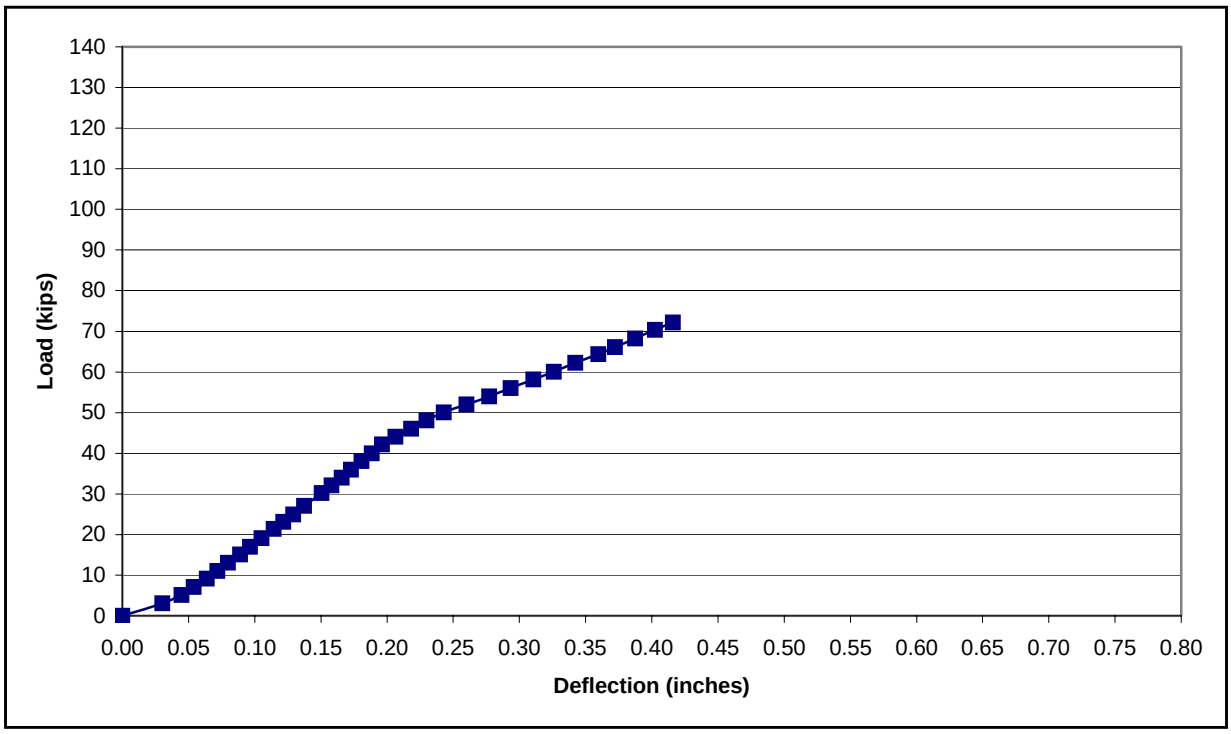

Figure C 3 Unadjusted Load Deflection Curve, Position 3

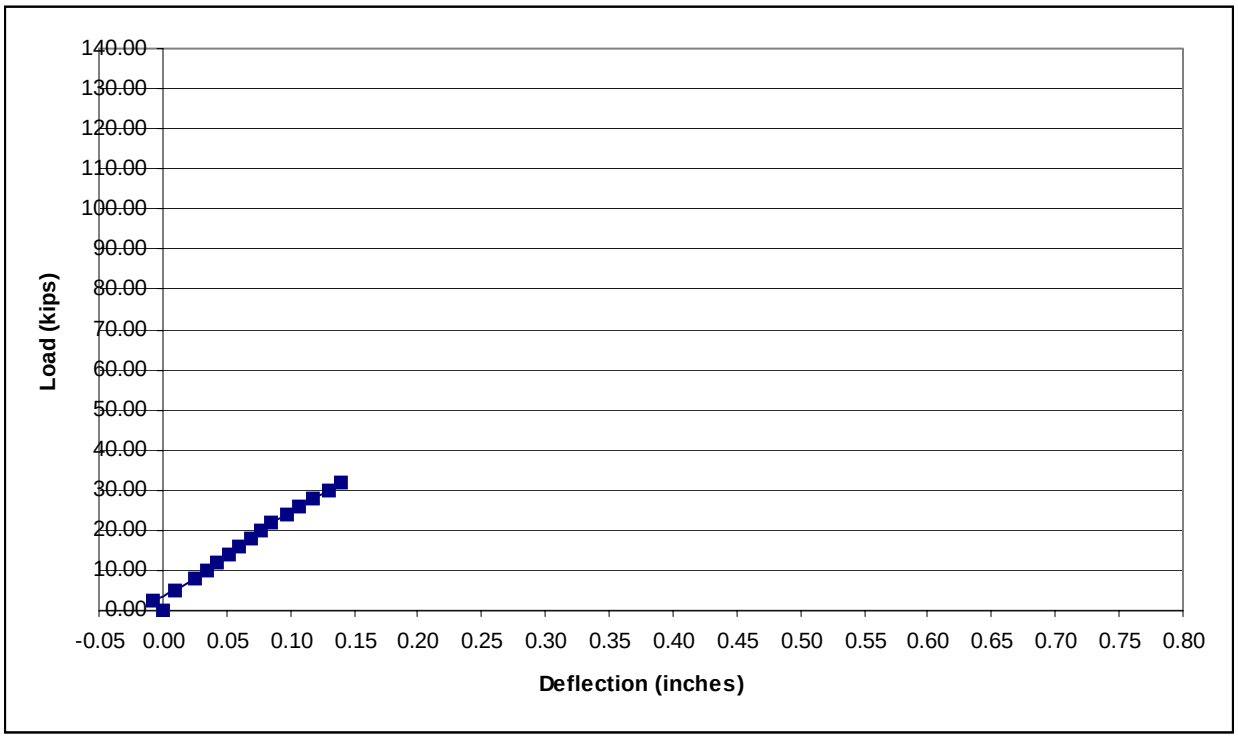

Figure C 4 Unadjusted Load Deflection Curve, Position 4

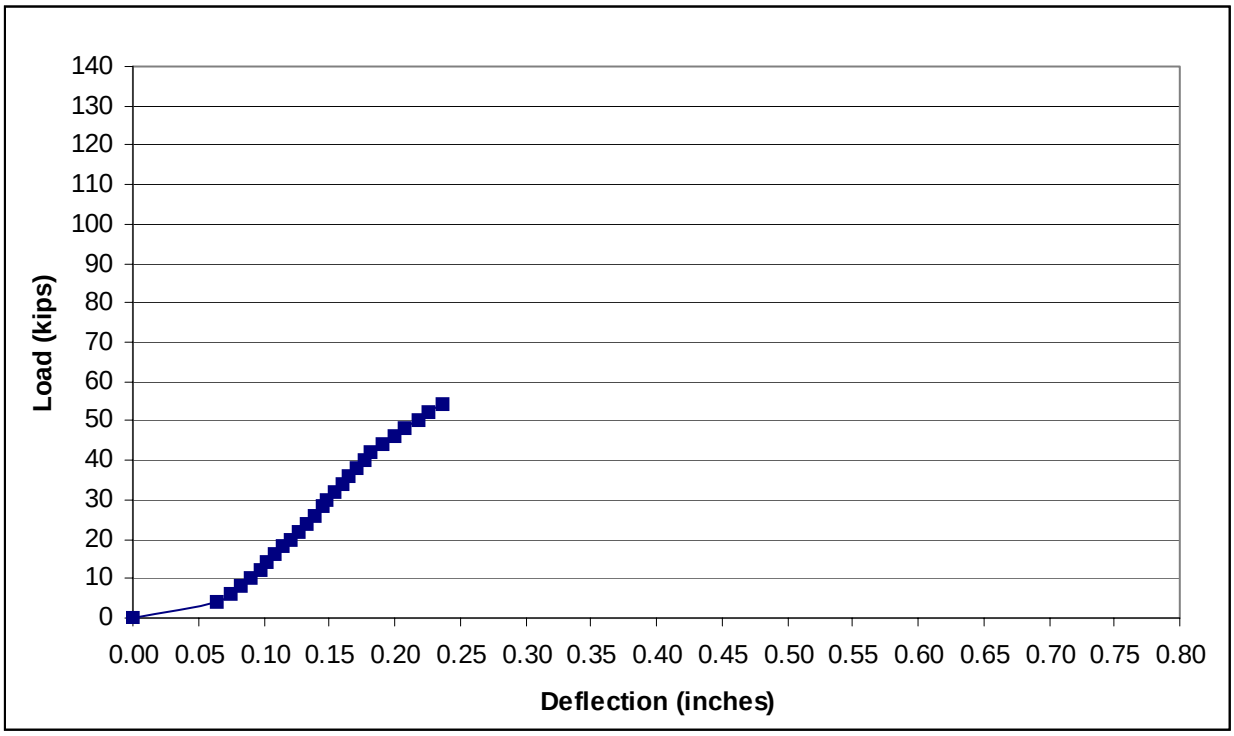

Figure C 5 Unadjusted Load Deflection Curve, Position 5

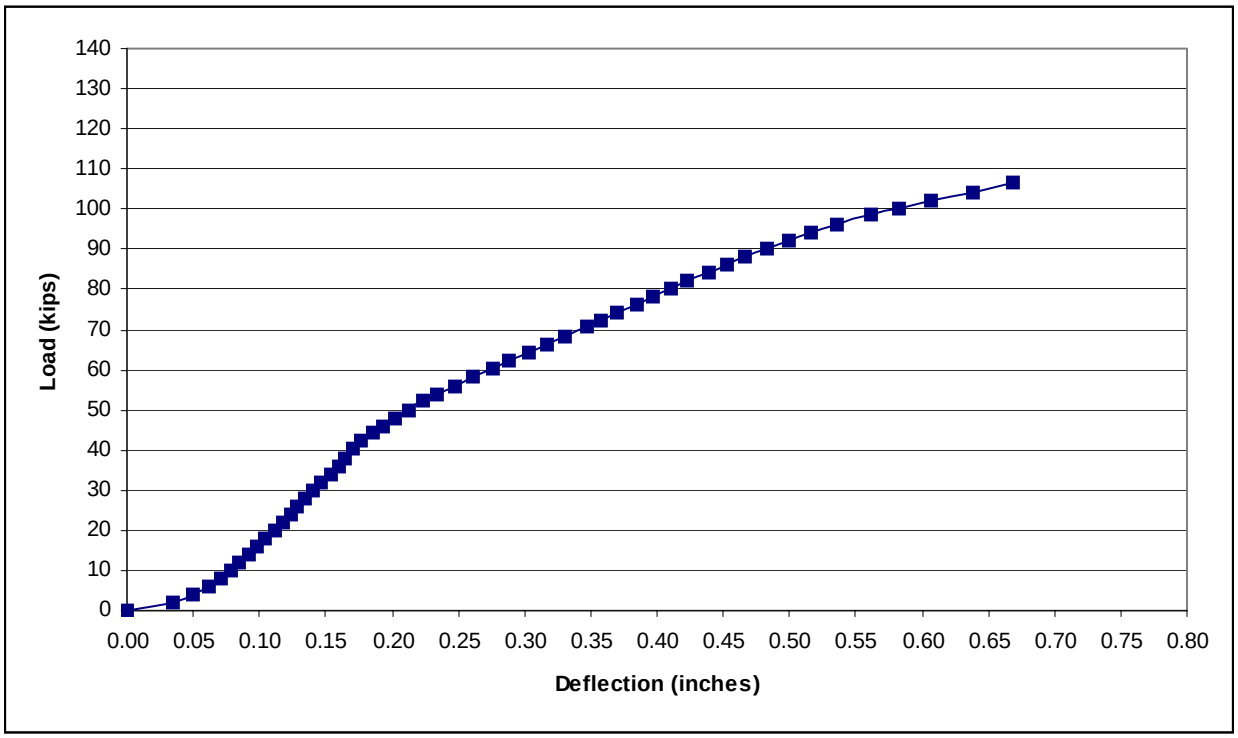

Figure C 6 Unadjusted Load Deflection Curve, Position 6a

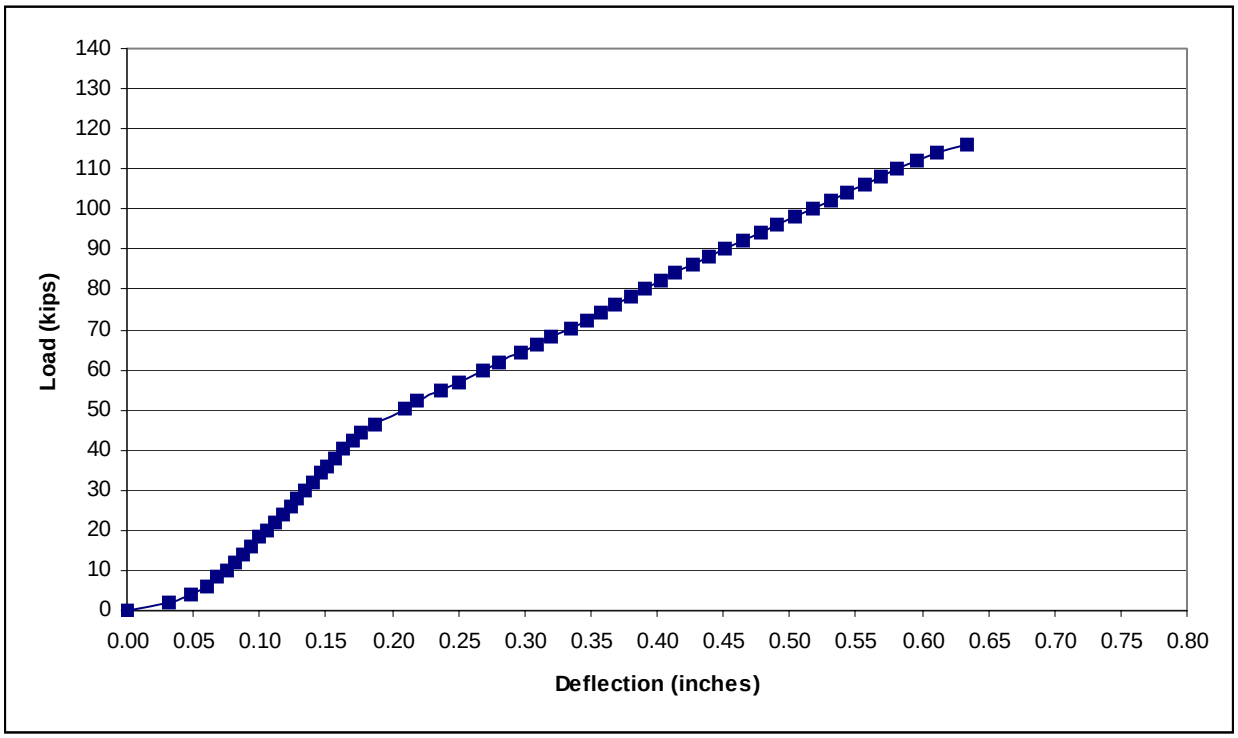

Figure C 7 Unadjusted Load Deflection Curve, Position 6b

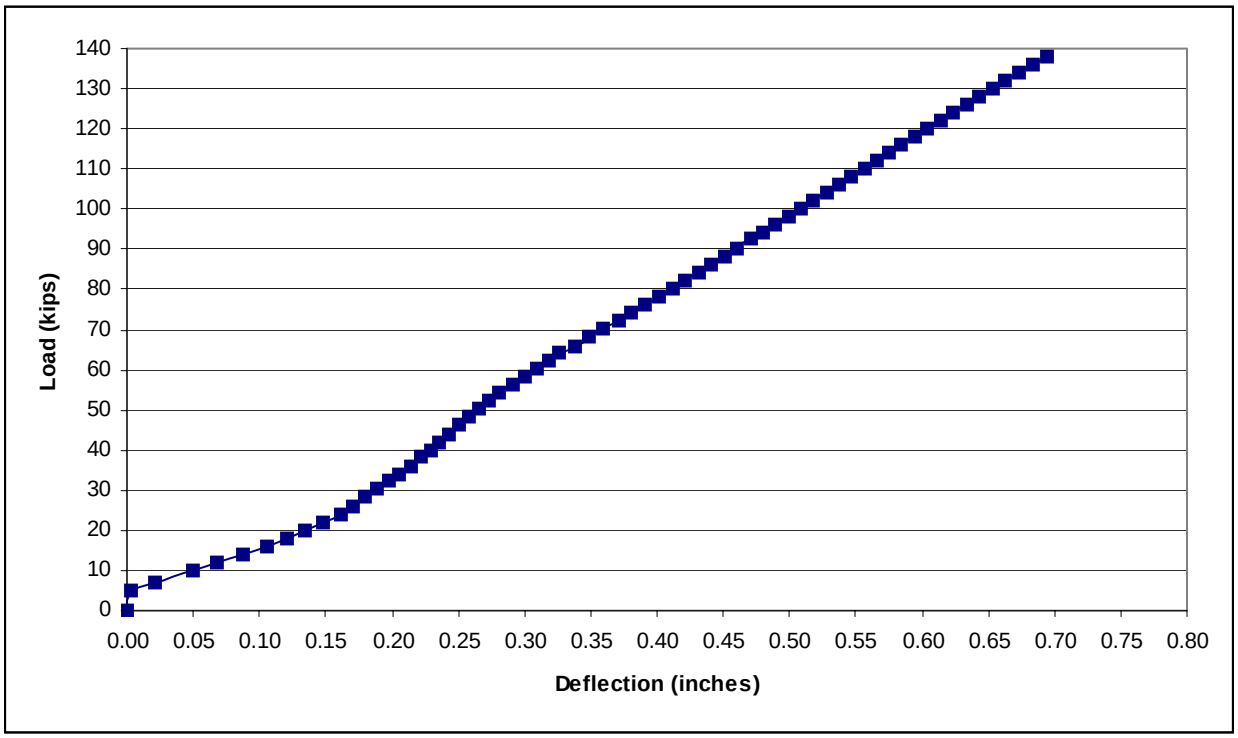

Figure C 8 Unadjusted Load Deflection Curve, Position 7

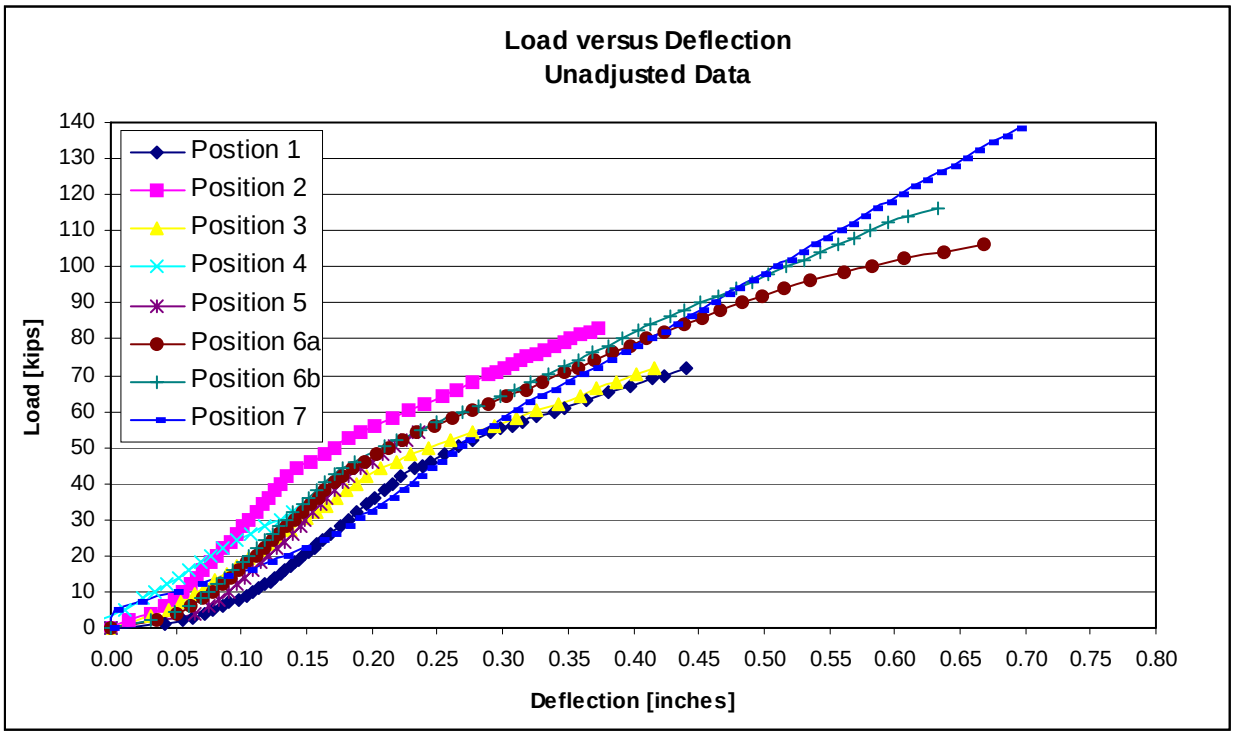

Figure C 9 Comparison of All Unadjusted Load Deflection Curves

APPENDIX D

ADJUSTED LOAD DEFLECTION CURVES

Each of the three plots in this appendix reflects adjustments made to the raw data presented in Section 3.5. For testing positions 1 through 5, where a three-inch plate was substituted for the one-inch plate used, it should be noted that the thicker plate would more evenly distribute the applied load over the contact surface with the FRP deck panel, enabling the testing position to accumulate larger loads and subsequently higher ultimate load capacities. In Figure D 3, the curves for testing positions 1 through 5 are inaccurately shown because of the inability to predict the ultimate load capacity associated with the change in the thickness of the steel test pad.

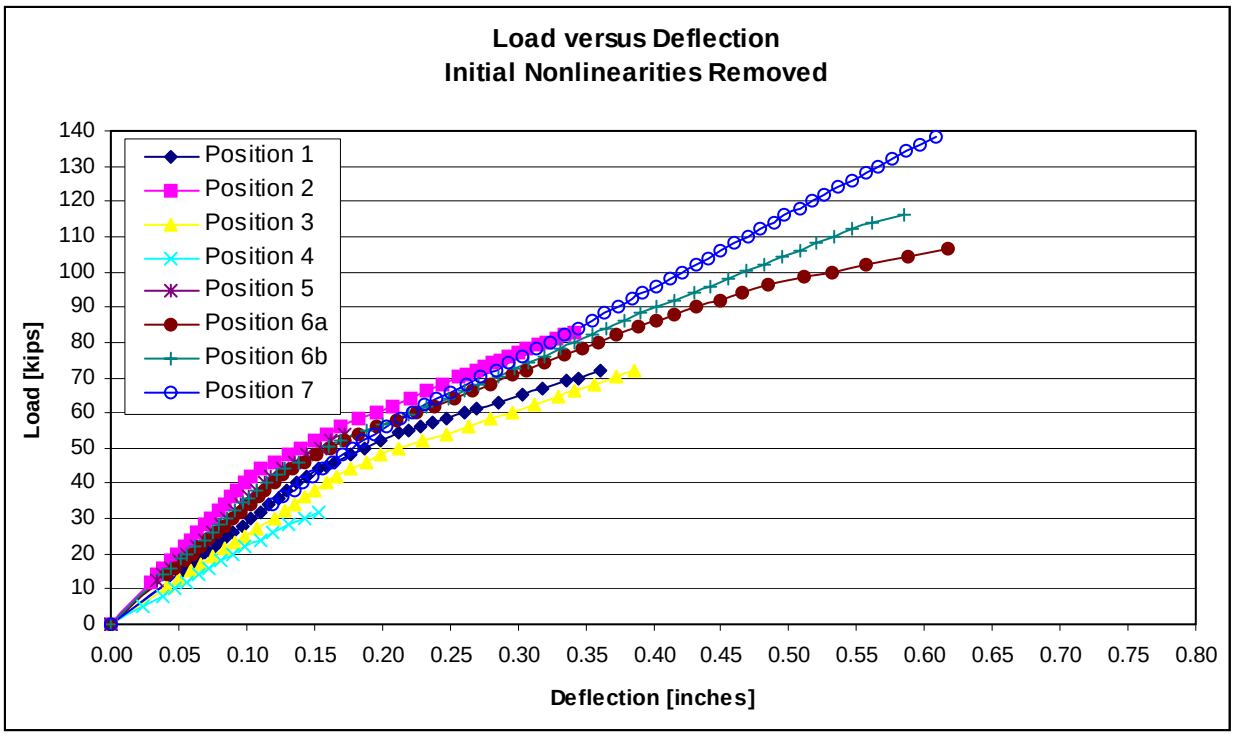

Figure D 1 Load Deflection Curves with Initial Nonlinearities Removed

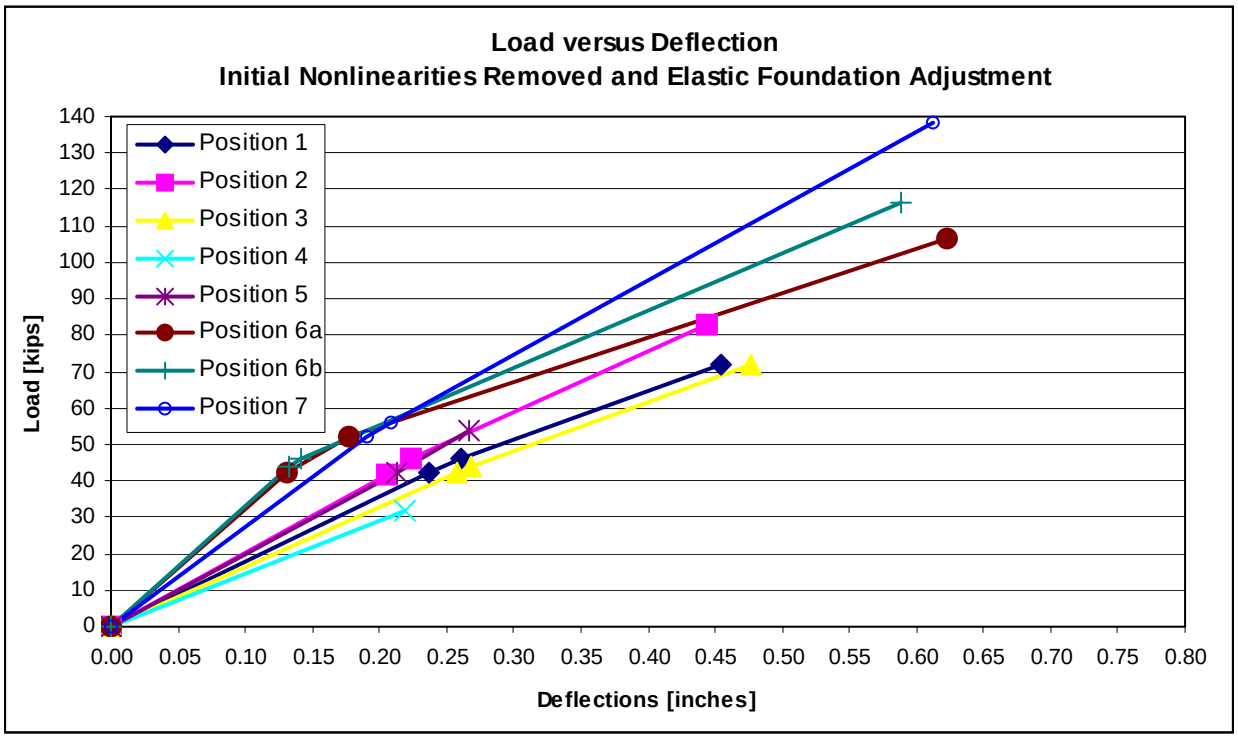

Figure D 2 Load Deflection Curves with Initial Nonlinearities Removed and Beam on Elastic Foundation Adjustment

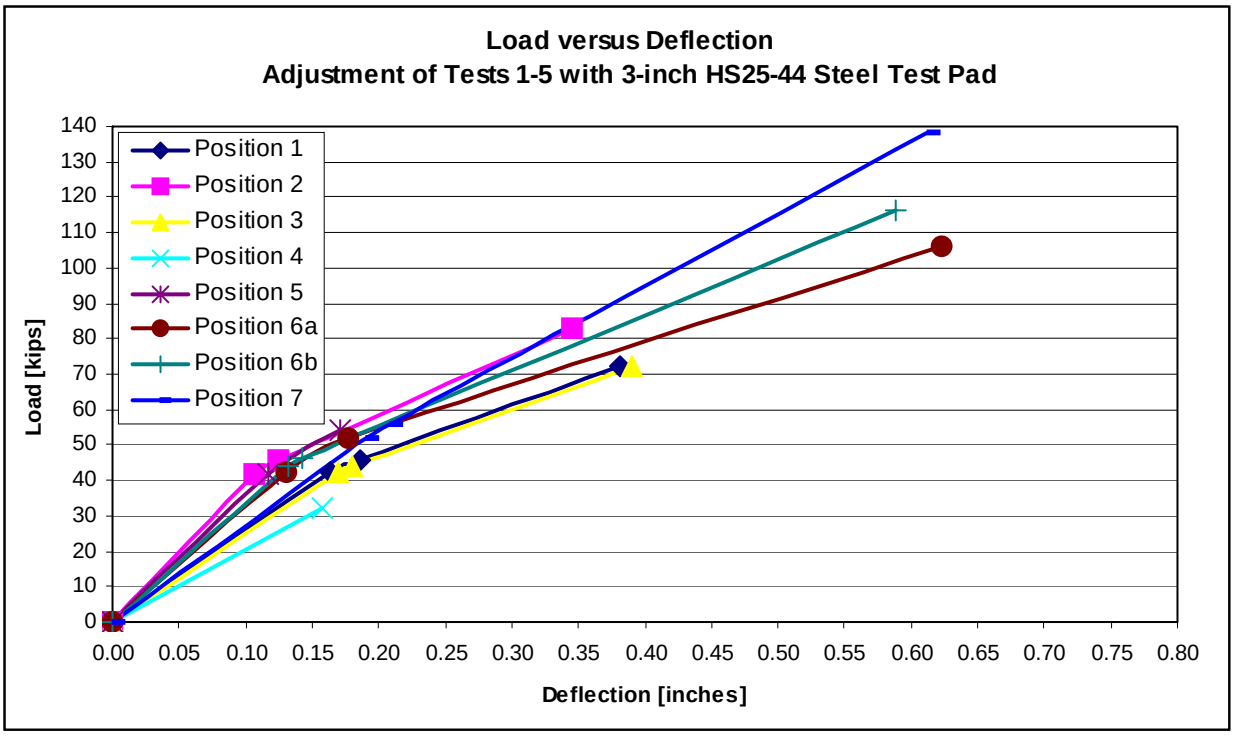

Figure D 3 Load Deflection Curves with Hypothetical 3-inch Thick Plate Model

APPENDIX E

STRESS STRAIN RELATIONSHIPS

The stress strain relationships are presented for each of testing position with the unadjusted and adjusted data. The unadjusted curves are from the data in Appendix B, and the adjusted curves are from Figure D 3.

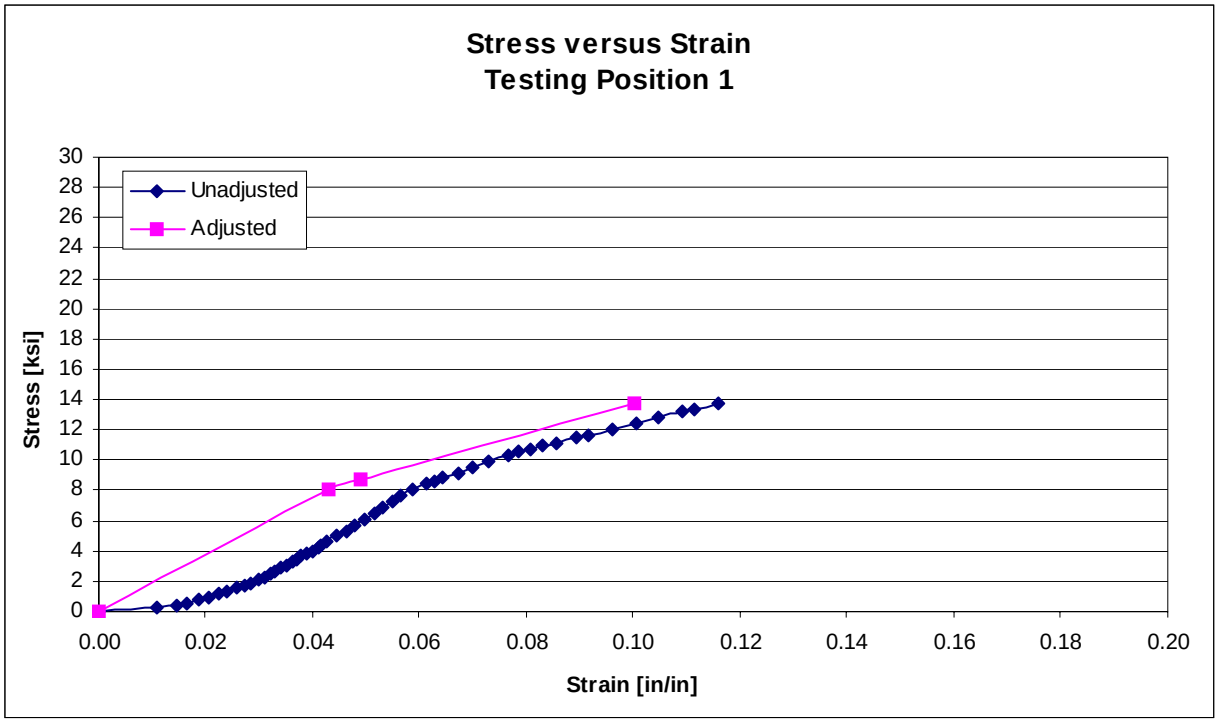

Figure E 1 Stress Strain Curves For Testing Position 1

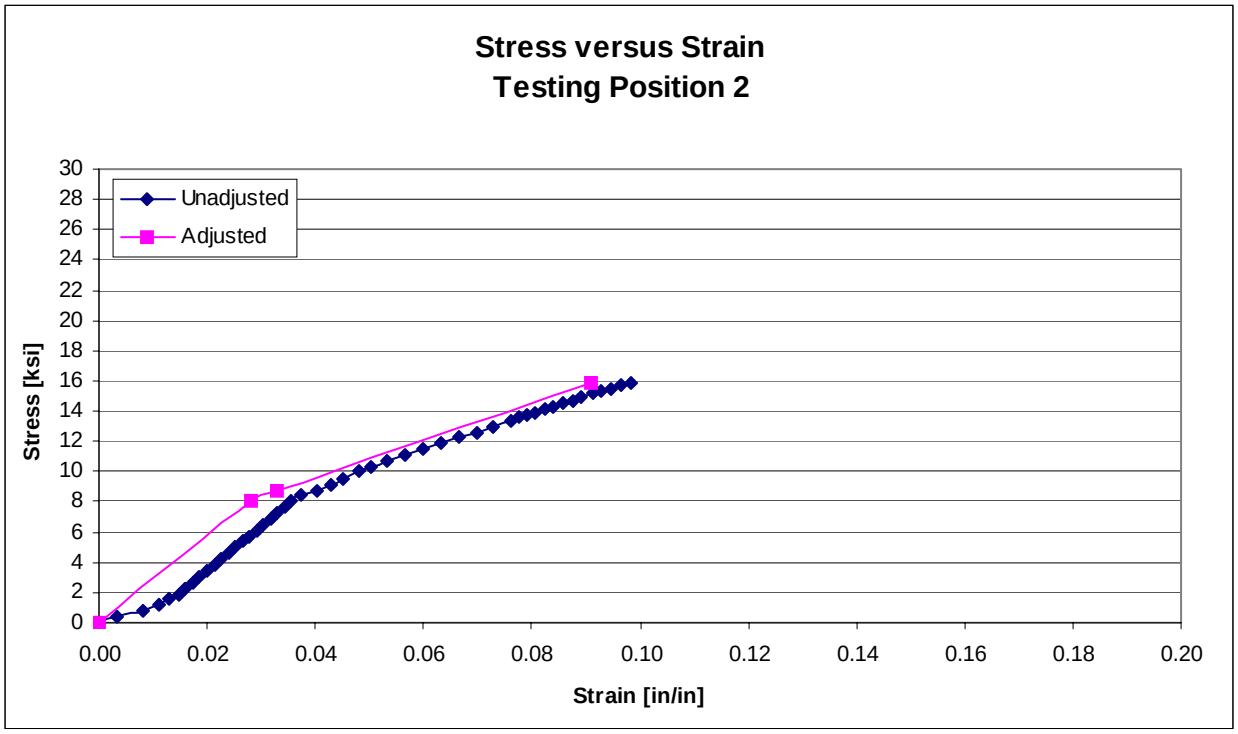

Figure E 2 Stress Strain Curves For Testing Position 2

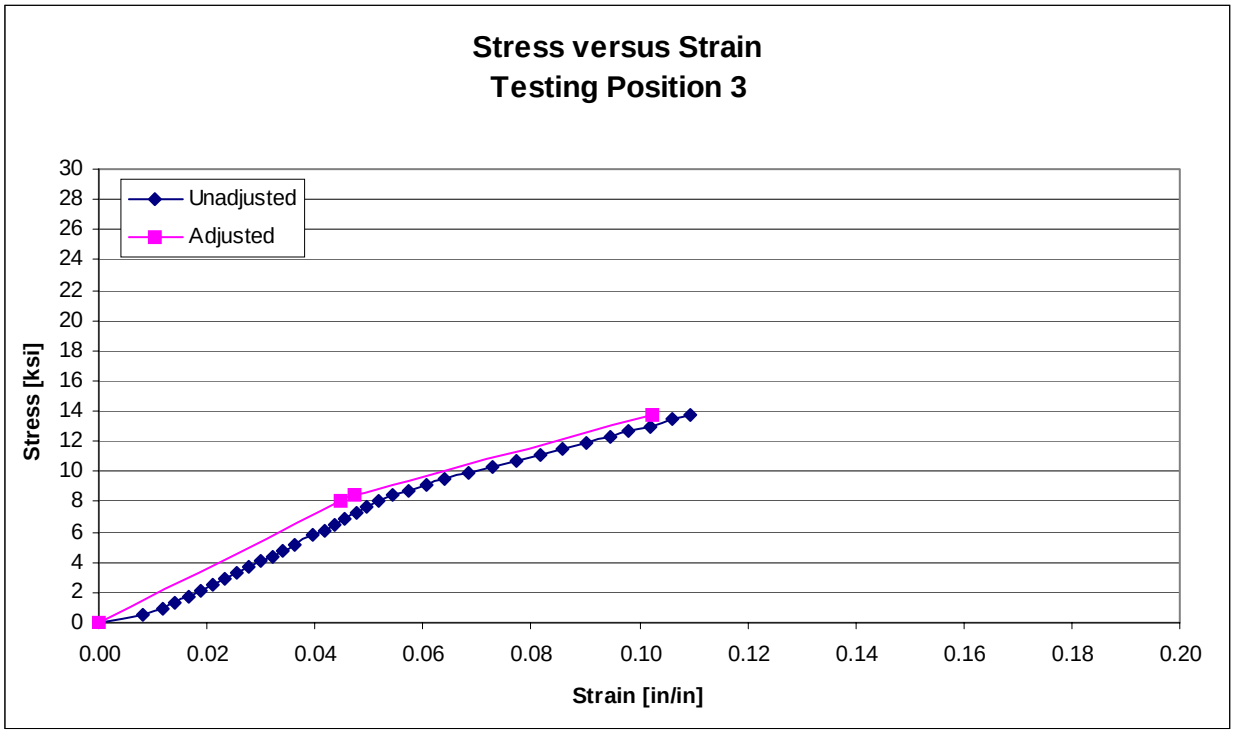

Figure E 3 Stress Strain Curves For Testing Position 3

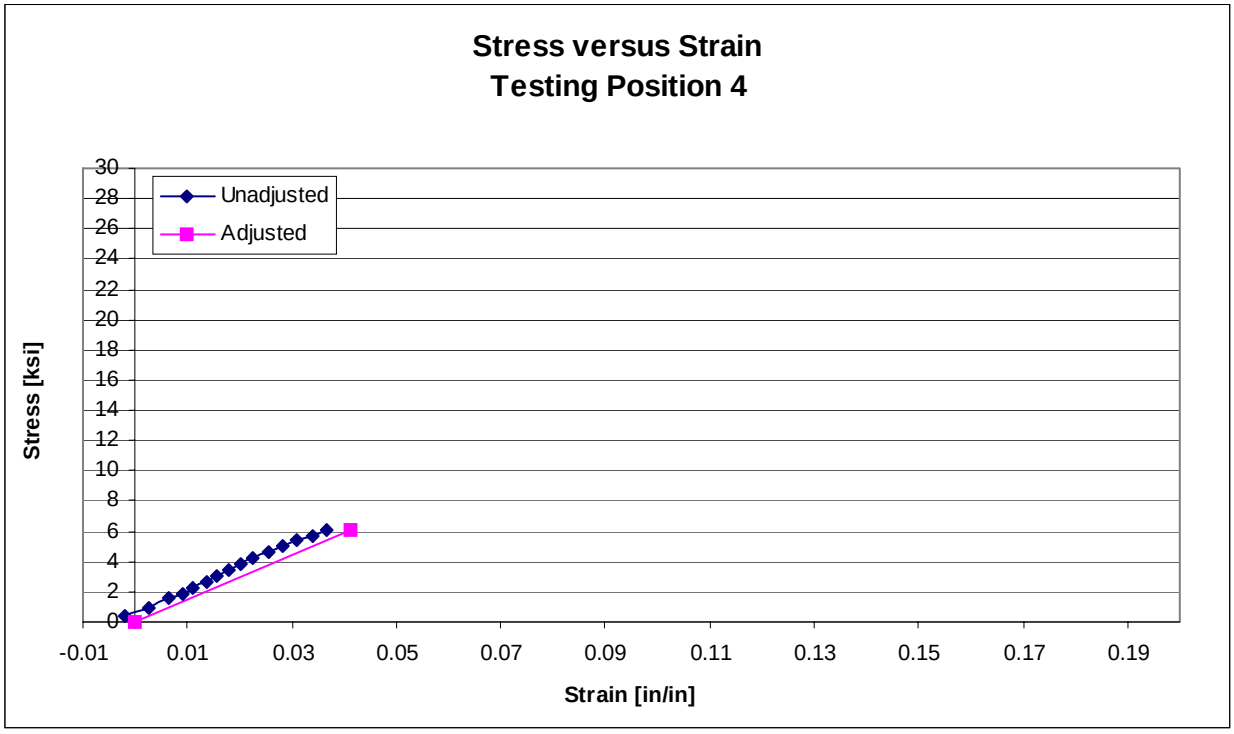

Figure E 4 Stress Strain Curves For Testing Position 4

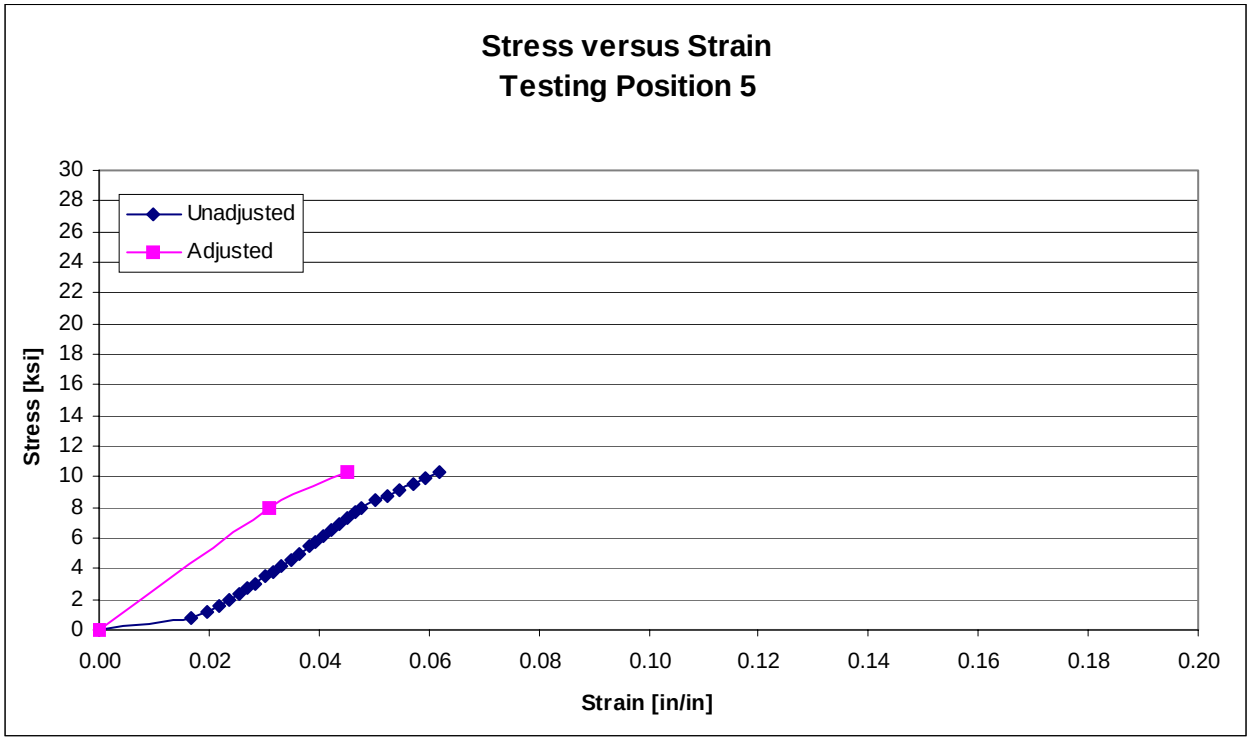

Figure E 5 Stress Strain Curves For Testing Position 5

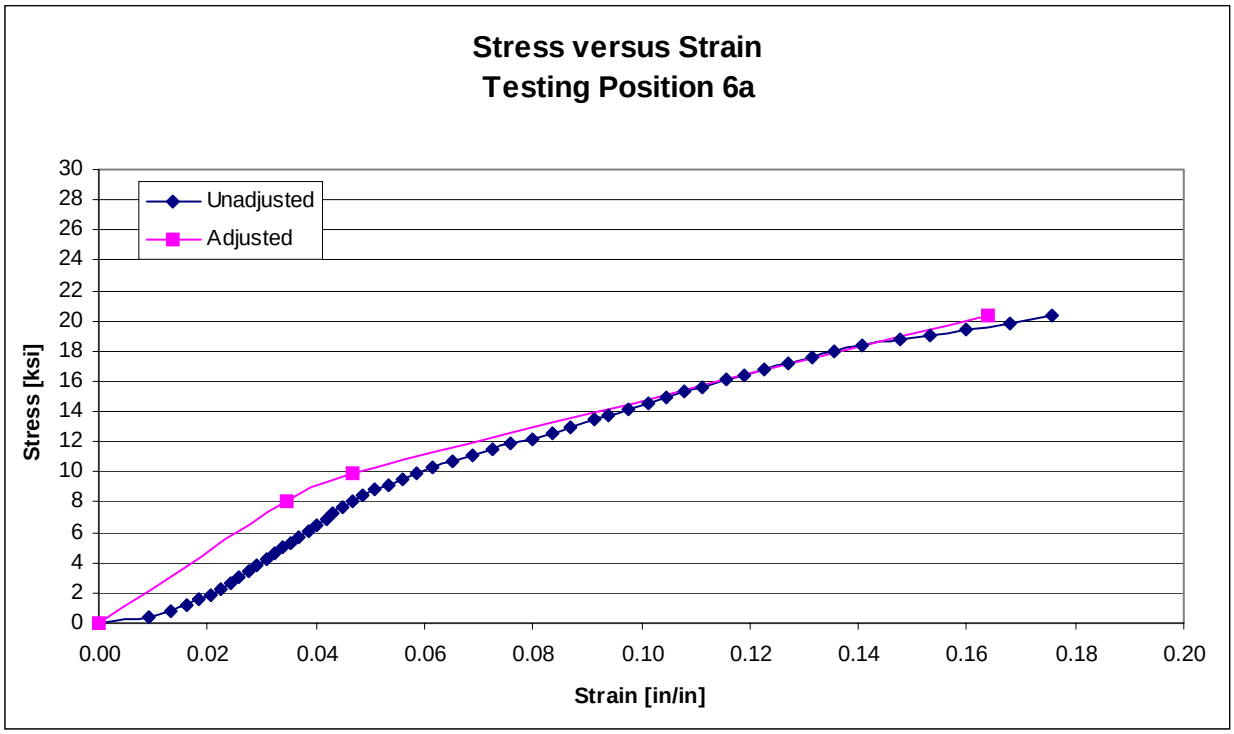

Figure E 6 Stress Strain Curves For Testing Position 6a

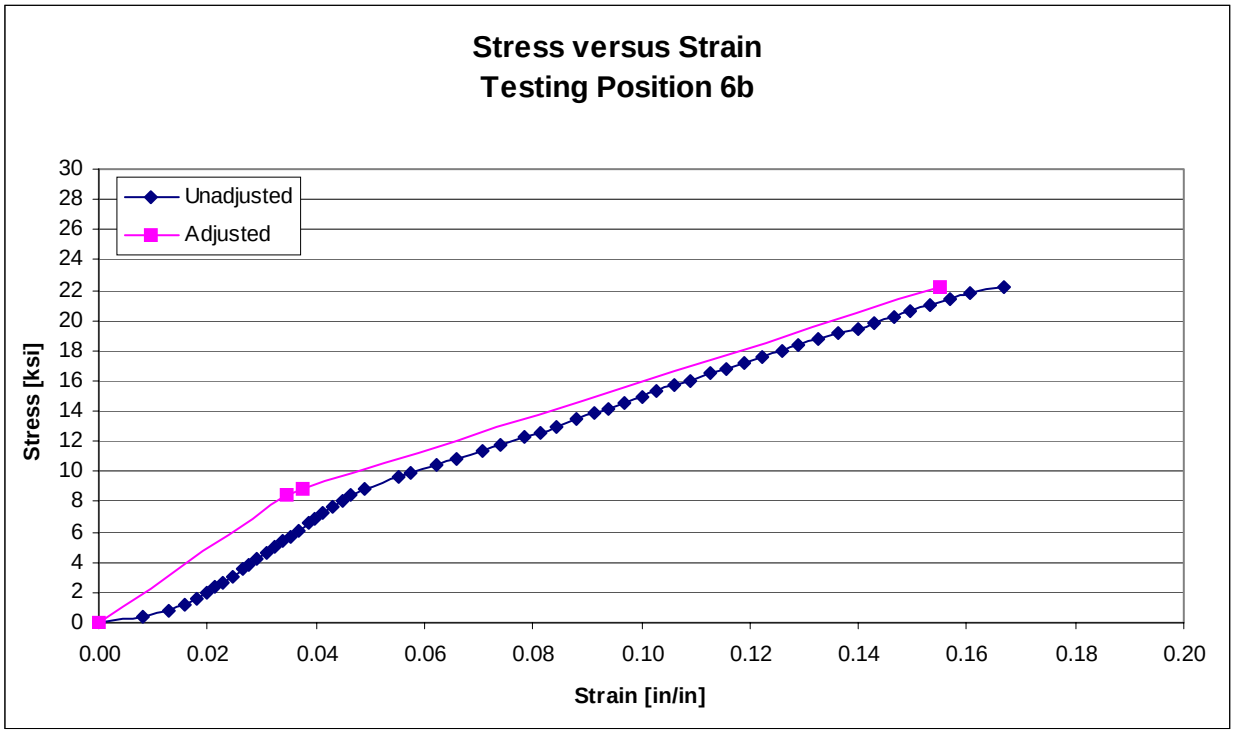

Figure E 7 Stress Strain Curves For Testing Position 6b

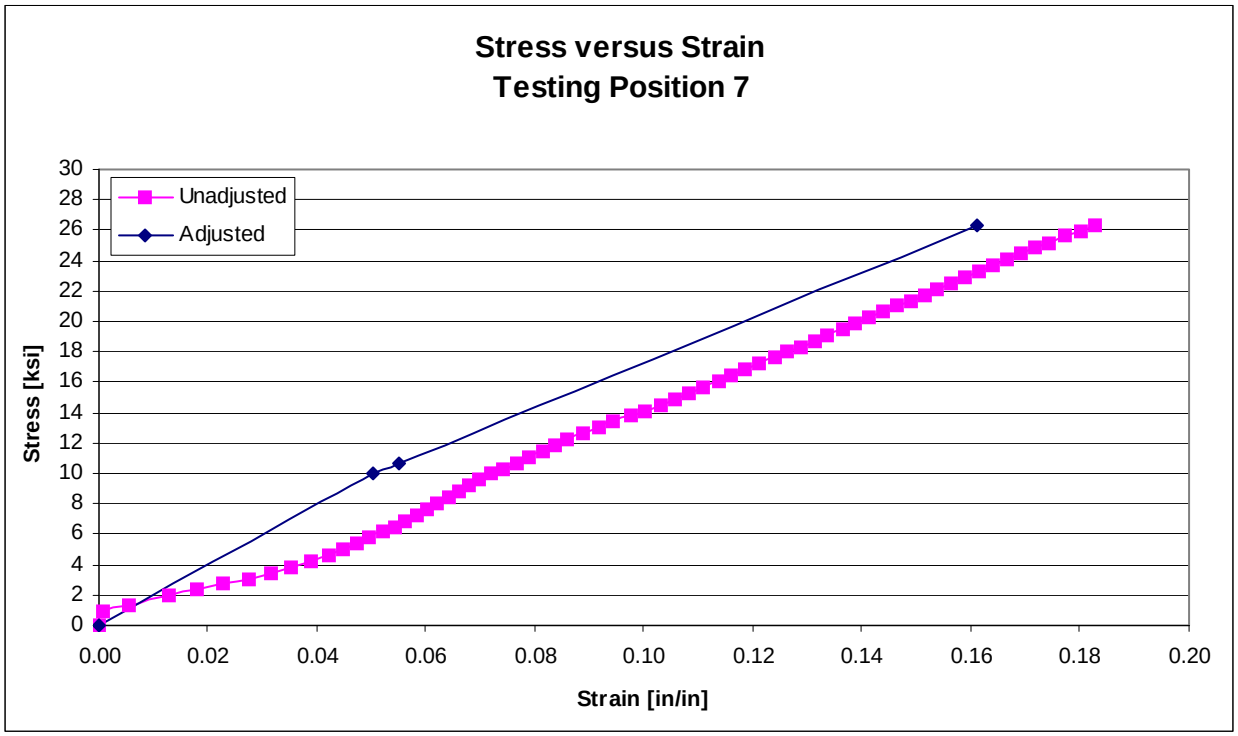

Figure E 8 Stress Strain Curves For Testing Position 7

APPENDIX F

BEAM ON ELASTIC FOUNDATION MODEL

After the initial nonlinearities were removed from the data original data (see Figure D 1), Hetényi's beam on elastic foundation model was employed to adjust the measured deflection at the end of the plate to the true deflection at the center of the plate (see Figure D 3). In our model, the HS25-44 test pad was modeled as the beam, and the FRP web and flanges were modeled as the elastic foundation. Determining the modulus of the foundation was difficult, because of the complexity of the makeup of the FRP. By inspection of Equation F 2, the only unknown is the modulus of the foundation, k_0, embedded in β and k. Since the adjusted deflection at the end of the plate is known at a particular applied load, the modulus of the foundation can be found using trial and error. Once the modulus of the foundation is calculated for the particular testing position, the deflections at the center of the plate can be calculate via equation F 1.

To model the loading conditions in the experimental testing, Hetényi's short beam on an elastic foundation (as described by Boresi and Schmidt) with a concentrated force at midspan was used. The deflections at the midspan and at the end of the beam are given in Equations F 1 and F 2.

$$y_C = \frac{P\beta}{2k} \cdot \frac{\cosh(\beta L) + \cos(\beta L) + 2}{\sinh(\beta L) + \sin(\beta L)} \quad \text{(F 1)}$$

$$y_e = \frac{2P\beta}{k} \cdot \frac{\cosh(\frac{\beta L}{2}) + \cos(\frac{\beta L}{2})}{\sinh(\beta L) + \sin(\beta L)} \quad \text{(F 2)}$$

where,

$$\beta = \sqrt[4]{\frac{k}{4EI}} \quad \text{(F 3)}$$

$$k = bk_O \quad \text{(F 4)}$$

$$I = \frac{bh^3}{12} \quad \text{(F 5)}$$

EI ≡ flexural rigidity of plate [kip-in^2]

k_o ≡ modulus of FRP deck (foundation) [ksi]

b ≡ constant width of plate in contact with FRP deck (foundation) [in]

l ≡ length of plate [in]

h ≡ thickness of plate [in]

P ≡ applied load [kips]

The following is the computer code, with the most significant outputs of the model are the calculation of the modulus of the FRP deck section and the deflection at the center of the plate.

```
1  clc;
2  clear;
3
4  %input values for the dimensions of the plate
5  %input values for plate properties
6  %input values for the dimensions for the web
7  %input value for applied load
8  l  = input('What is the length of plate (l) [in]:   ');
9  w  = input('What is the width of plate (w) [in]:   ');
10 t  = input('What is the thickness of plate (t) [in]:   ');
11 E  = input('What is the modulus of plate (E) [ksi]:   ');
12 P  = input('What is the load (P) [kips]:   ');
13 tw = input('What is the thickness of FRP web (tw) [in]:   ');
14 lw = input('What is the length of FRP web (lw) [in]:   ');
15
16 %input values from actual test measurement data
17 Disp('What is the measured value of the modulus');
18 Ef = input('         from the bearing test (Ef) [ksi]:     ');
19 dt = input('What is the measured deflection at load P: (dt) [in]:
   ');
20 tn = input('What is the number of the test:  ','s');
21 clc;
22
23 %display header for output file
24 [x,y]=size(tn);
25 disp(['-----------------------------------------------------------
   --------']);
26 if y == 2
27     disp(['-----This is the data for Position ', tn, ' of the FRP
       bearing tests-----']);
28 Else
29     disp(['------This is the data for Position ', tn, ' of the FRP
       bearing tests-----']);
30 End
31
32 disp(['-----------------------------------------------------------
   --------']);
```

```
33  Disp('  ')
34
35  %display of inputted data
36  Disp('The input values are: ');
37  Disp('  ');
38  disp(['l = ',num2str(l),' in   t = ',num2str(t),' in  w =
    ',num2str(w), ' in']);
39  disp(['E = ',num2str(E),' ksi   P = ',num2str(P),' kips   tw =
    ',num2str(tw), ' in']);
40  disp(['lw = ',num2str(lw),' in  dt = ',num2str(dt), ' in  Ef =
    ',num2str(Ef), ' ksi']);
41  Disp('  ');
42
43  %input modulus of foundation
44  ko = input('What is modulus of FRP (ko) [k/in^3]:   ');
45
46  %determination of moment of interia of plate
47  %determination of spring constant and beta value
48  I = w*t^3/12;
49  k = tw*ko;
50  Beta = (k/4/E/I)^(1/4);
51
52  %determination if analysis is a(n) valid/invalid short beam model
53  if l < 3*pi/2/beta
54      disp('  ');
55      disp('VALID for short beams');
56      disp('  ');
57  Else
58      disp('  ');
59      disp('INVALID for short beams');
60      disp('  ');
61  End
62
63  %displacement at the center of the plate
64  y_center = (P * beta / 2 / k ) * (cosh(beta*l) + cos(beta*l)+2) /
    (sinh(beta*l) + sin(beta*l));
65
66  %displacement at the end of the plate
67  y_end = (2 * P * beta / k) * (cosh(beta*l/2) * cos(beta*l/2)) /
    (sinh(beta*l) + sin(beta*l));
```

```
68
69  %error analysis of displacements at end of the plate
70  percent_error = (dt - y_end)/y_end*100;
71
72  %output of displacements and error
73  disp(['Deflection at the center is:        ', num2str(y_center), '
    inches']);
74  disp(['Deflection at the ends are:         ', num2str(y_end), '
    inches']);
75  disp(['Percent error of end deflections:  ', num2str
    (percent_error),' %']);
76  Disp('   ');
77
78  %loop to increment modulus of foundation (FRP) to minimize
79  %the percent error of the deflections at the end of the plate
80  count = 0;
81  doagain=1;
82  while doagain==1
83      if abs(percent_error) < 0.01
84          doagain = 2;
85      Else
86          count = count + 1;
87          %increment/decrement modulus of foundation (FRP)
88          if percent_error > 0
89              ko = ko - 0.001;
90
91          Else
92              ko = ko + 0.001;
93          End
94
95          k = tw*ko;
96          beta = (k/4/E/I)^(1/4);
97          y_end = (2 * P * beta / k) * (cosh(beta*l/2) *
            cos(beta*l/2)) / (sinh(beta*l) + sin(beta*l));
98          percent_error = (dt – y_end)/y_end*100;
99
100         %display only every tenth error calculation
101         if mod(count,10) == 0
102
103             disp('   ');
```

```
104             disp(['Percent error of end deflections:  ',
                num2str(percent_error),' %']);
105             doagain=1;
106         End
107
108     End
109
110 End
111 Disp('   ');
112
113 %final header display of calculated values from model
114 disp('-----------------------------------------------------------
    -------');
115 disp('---Now we are going to compute the Youngs Modulus of the FRP
    web---');
116 disp('-----------------------------------------------------------
    -------');
117 Disp('  ')
118 Disp('  ')
119
120 %final calculation of values
121 E_FRP = ko * lw;
122 modulus_error = (Ef - E_FRP)/E_FRP*100;
123 y_center = (P * beta / 2 / k ) * (cosh(beta*l) + cos(beta*l)+2) /
    (sinh(beta*l)+sin(beta*l));
124
125 %final display of calculated values from model
126 Disp('At the applied load');
127 disp(['  the deflection at the center of the plate is:
    ',num2str(y_center), ' in']);
128 Disp('  ');
129 disp(['The measured value of Youngs Modulus is:
    ',num2str(Ef), ' ksi']);
130 disp(['The calculated value of Youngs Modulus is:
    ',num2str(E_FRP), ' ksi']);
131 disp(['The percent error is:                              ',
    num2str(modulus_error), ' %']);
132
133 %end of program footer
134 Disp('  ');
135 Disp('  ');
```

```
Disp('-------------------------------------');
Disp('-----------End of Program-----------');
Disp('-------------------------------------');
```

APPENDIX G

DEVELOPMENT OF PLASTIC HINGE

The development of the plastic hinge in the steel tests pads during testing positions 1 through 5 had a significant effect on the thickness of the steel test pads used during the testing of positions 6a, 6b, and 7. From mechanics of materials (Hibbler 2000), the plastic hinge was formed at the plastic moment M_p. M_p for a rectangular cross section is given in equation G-1.

$$M_p = \frac{bh^2}{4}\sigma_y \qquad \text{(G 1)}$$

where,

b ≡ width of beam [in]

h ≡ depth of beam [in]

σ_y ≡ yield strength of beam [ksi]

To determine the load that is required to cause M_p, basic statics analysis must be performed on the free body diagram of the plate, before the last increment of loading that caused M_p. For the free body diagram, there was an applied concentrated load at the center of the plate and a reaction normal force due to the contact of the footprint with the FRP deck. Because of symmetry, only one side of the plate will be analyzed. From the free body diagram, the M_{max} in

the plate occurred at a distance of L/4 from the center of the plate and was found by the following:

$$M_{\max} = \frac{P}{2} \cdot \frac{L}{4} = \frac{PL}{8} \qquad \text{(G 2)}$$

where,

P ≡ load to cause plastic hinge [kips]

L ≡ length of beam [in]

Now substituting Equation G 1 into Equation G 2 and solving for P yields Equation G 3.

$$P = \frac{8M_p}{L} = \frac{2\sigma_y bh^2}{L} \qquad \text{(G 3)}$$

Table G 1 summarizes values of plastic moment and load required to initiate the plastic hinge in the flexible (h = 1 inch) and rigid (h = 3 inches) steel test pads for A36 steel.

Table G 1 Plastic Moment and Required Load to Initiate Plastic Hinge in Testing Plates

Plate Type	Plastic Moment, M_p [kip-in]		Required Load, P [kips]	
	36 ksi	60 ksi	36 ksi	60 ksi
Flexible, 1-inch	90	150	36	60
Rigid, 3-inch	810	1350	324	540

BIBLIOGRAPHY

American Association of State Highway and Transportation Officials (AASHTO), (1996). Sixteenth Edition.

Austin, C., (2002). *Buckling of Symmetric Laminated Fiberglass Reinforced Plastic (FRP) Plates.* Master's Thesis, Civil and Environmental Engineering. University of Pittsburgh. Pittsburgh, PA.

Boresi, A.P., and Schmidt, R.J., (2003). *Advanced Mechanics of Materials.* Sixth Edition, John Wiley & Sons, Inc. New York, NY.

Cassity, P.A. (2000). "Fiber-Reinforced Polymer Bridge Decks". *National Bridge Research Organization (NaBRO).* http://www.nabro.unl.edu/articles/20000805.

Ehlen, M.A., (1999). "Life-cycle Costs of Fiber-Reinforced-Polymer Bridge Decks". *Journal of Materials in Civil Engineering*. Volume 11, Number 3, August 1999.

Federal Highway Adminstration (FHWA), (1997). "Advanced Composites in Europe and Japan". *U.S. Department of Transportation.*

Federal Highway Administration (FHWA), (2003). "National Bridge Inventory Data". *U.S. Department of Transportation*.

Hetenyi, M., (1946). *Beams on Elastic Foundation: Theory with Applications in the Fields of Civil and Mechanical Engineering.* Ann Arbor: University of Michigan Press. Ann Arbor, MI.

Hibbler, R.C., (2000). *Mechanics of Materials.* Fourth Edition. Prentice Hall, Inc. Upper Saddle River, NJ.

Luo, Y., Keelor, C., Yulismana, W., Earls, C.J., (2002). "Field Monitoring of the Boyer Bridge Fiber Reinforced Polymer Deck Installation". *Proceedings of the International Bridge Conference*, Pittsburgh PA paper IBC-02-52 CD-ROM.

Nystrom, H., Watkins, S., Nanni, A., and Stone, D.K., (2002). "Laboratory and Field Testing of FRP Composite Bridge Decks and FRP-Reinforced Concrete Bridge For City of St. James, Phelps County, MO". *Missouri Department of Transportation.*

Market Development Alliance (MDA) of FRP Composite Industry, (2000). *Product Selection Guide: FRP Composite Products for Bridge Applications.* First Edition.

Scott, I. and Wheeler, K., (2001). "Application of Fibre Reinforced Polymer Composites in Bridge Construction". *Institution of Public Works Engineering Australian*, Second Conference.

Taly, N., (1998). *Design of Modern Highway Bridges.* McGraw-Hill Company, Inc. New York, NY.

Texas Department of Transportation (TXDOT), (2001), *2001 Bridge Design Manual*. Manual Notice 2000-1.

Yulismana, W., (2004). *Experimental Testing to Evaluate Performance of 5-inch Fiber Reinforced Polymer (FRP) Decks When Mechanically Attached to Steel Stringer(s).* Ph.D. Dissertation, Civil and Environmental Engineering. University of Pittsburgh, Pittsburgh, PA.